

# A Time Marching Boundary Element Method for the Prediction of the Flow Around Surface Piercing Hydrofoils

by

Cedric Marcel Savineau

B.S. Mechanical Engineering University of Massachusetts, Amherst, 1993

Submitted to the Department of Ocean Engineering and the Department of Mechanical Engineering in partial fulfillment of the requirements for the degree of

Master of Science in Ocean Engineering and

Master of Science in Mechanical Engineering

at the

MASSACHUSETTS INSTITUTE OF TECHNOLOGY

February 1996

© Massachusetts Institute of Technology, 1996. All Rights Reserved.

Author .....

Department of Ocean Engineering and  
Department of Mechanical Engineering  
January 26, 1996

Certified by .....



Spyros A. Kinnas

Lecturer, MIT, Department of Ocean Engineering

Assistant Professor of Civil Engineering, University of Texas at Austin

Thesis Supervisor



Certified by .....

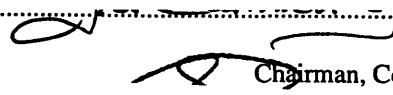


Ahmed F. Ghoniem

Professor of Mechanical Engineering

Thesis Reader

Accepted by .....



Douglas Carmichael

Chairman, Committee on Graduate Students

Accepted by .....



Ain A. Sonin

Chairman, Department Committee on Graduate Students

MASSACHUSETTS INSTITUTE  
OF TECHNOLOGY

APR 16 1996



LIBRARIES



# **A Time Marching Boundary Element Method for the Prediction of the Flow Around Surface Piercing Hydrofoils.**

by

Cedric Marcel Savineau

Submitted to the Department of Ocean Engineering and the Department of Mechanical Engineering on January 26 1996, in partial fulfillment of the requirements for the degree of Master of Science in Ocean Engineering and Master of Science in Mechanical Engineering.

## **Abstract**

The flow field around a fully ventilated two-dimensional surface piercing hydrofoil is considered. The problem is treated using nonlinear theory by employing a low-order potential-based boundary-element method. The solution can be divided in two parts: (1) initial entry when the foil is only partially submerged, (2) complete entry, when the foil is fully submerged under the free surface.

The presented theory is a time domain panel method, where the perturbation potential on the cavity surface is a function of submergence and time. As the foil cuts through the free surface during its motion, the potential on the discretized leading edge cavity panel, remains at the location when it was generated. The source strengths on the wetted part of the foil are known from the kinematic boundary condition. From continuity at the leading edge and trailing edge of the foil, the dipole strengths on the cavity are also known from the previous timestep. However, since the dipole strengths on the wetted part of the foil are unknown, the dipole strengths on the cavity can be integrated in the solution procedure.

The non-linear cavity geometry is determined iteratively within the solution by enforcing the kinematic boundary condition on the exact cavity surface at each timestep. A linearized free surface condition is enforced by using the image method. The image sources and dipoles are of opposite strength to those of the submerged foil and cavity. This results in a zero horizontal perturbation velocity on the free surface.

The developed analysis is shown to be robust and to produce convergent results with increasing number of panels and with number of iterations per timestep. Pressure distributions compare favorably with linear theory at small angles of attack and low camber to chord ratios. At higher angles of attack the non-linear effects become more predominant. The non-linear cavity thickness is always considerably smaller than predicted from analytical linear methods.

The method developed here can directly be applied to the analysis of partially submerged supercavitating propellers.

Thesis Supervisor: Spyros A. Kinnas

Title: Lecturer, MIT, Department of Ocean Engineering and Assistant Professor of Civil Engineering, University of Texas at Austin

# Acknowledgments

I am grateful to many people for their support, advice, and friendship. First and foremost is my advisor, Prof. Spyros A. Kinnas, who has always encouraged and pushed me to achieve many ambitions and goals, that otherwise would not have been possible. He has always had time to advise and assist me in my research, and has always stuck with me, especially in difficult times. Special thanks go to Prof. Jake Kerwin and Dr. Dave Keenan, whose advise has very often made all the difference when I was at a standstill in my research. I also would like to thank all the “propeller nuts” for providing a unique and fun work environment.

Of course there is more to MIT than research, and I would like to thank all my friends for their moral support, and making life a whole lot brighter. I especially want to thank Wes, for his driving adventures, and Scott for his sailing commitment.

From the bottom of my heart, I want to thank my parents for always having supported, encouraged, and believed in me, especially a few years back, when no one else did. Most importantly, I would like to thank my wife Sylvie, for her everlasting love and timeless patience. She has always stood closely at my side through all the sweat and tears. I would never have made it this far without her. I dedicate this thesis to her.

This work was supported by an International Consortium on Cavitation Performance of High Speed Propulsors composed of the following fifteen members: Daewoo, DTMB, El Pardo MB, HSVA, Hyundai, IHI, KaMeWa, Mercury, Michigan Wheel, OMC, Rolla, Sulzer-Escher Wyss, Ulstein, Volvo-Penta, and Wartsila.

# Table of Contents

<b>1</b>	<b>Introduction.....</b>	<b>10</b>
1.1	Surface Piercing Hydrofoils and Propellers.....	10
1.2	Previous Research.....	11
1.3	Objectives of the Present Method.....	12
<b>2</b>	<b>Mathematical Formulation.....</b>	<b>14</b>
2.1	Overview.....	14
2.2	Potential Flow and Green’s Formula.....	14
2.3	Problem Definition.....	16
2.4	Boundary Conditions.....	17
2.5	Non-Linear Cavity Shape Determination.....	20
2.6	Pressures on the Foil and Cavity Surface.....	23
<b>3</b>	<b>Discrete Formulation.....</b>	<b>26</b>
3.1	Discretized Surface Piercing Foil Geometry.....	26
3.2	Discretized Green’s Formula.....	29
3.3	Free Surface Boundary Condition.....	30
3.4	Governing System of Equations.....	31
3.5	Non-Linear Cavity Shape Determination.....	43
3.6	Pressures on the Foil.....	45
<b>4</b>	<b>Numerical Validation.....</b>	<b>48</b>
4.1	Convergence.....	48
4.2	Comparisons with Other Methods.....	59
<b>5</b>	<b>Conclusions and Recommendations.....</b>	<b>64</b>
5.1	Conclusions.....	64
5.2	Recommendations and Future Work.....	65
	<b>Bibliography.....</b>	<b>68</b>



## List of Figures

Figure 2.1 Sketch of Hydrofoil in Unbounded Fluid.....	15
Figure 2.2 : Sketch of Surface Piercing Hydrofoil with Coordinate System Moving with the Foil .....	17
Figure 2.3 Vector diagram of cavity surface velocities before convergence.....	21
Figure 2.4 Sketch of cavity surface height update at each iteration .....	22
Figure 3.1 Discretized foil and cavity geometry. Panel indexing of foil and cavity for partially submerged chord length.....	26
Figure 3.2 Discretized foil and cavity geometry. Panel indexing of foil and cavity for full chord submergence .....	27
Figure 3.3 Discretized foil and cavity geometry. Panel indexing of foil and cavity for fully submerged stage.....	28
Figure 3.4 Discretized foil and cavity geometry. Panel indexing of foil and cavity at end of fully submerged stage .....	29
Figure 3.5 Perturbation Potential Distribution on Actual Foil and Cavity surface and Their Images .....	31
Figure 3.6 Iterative cavity surface determination .....	44
Figure 4.1 Convergence of upper cavity thickness growth with iterations per timestep.	48
Figure 4.2 Convergence of lower cavity thickness growth with iterations per timestep.	49
Figure 4.3 Cavity geometry convergence with iterations per timestep. ....	50
Figure 4.4 Cavity geometry convergence with iterations per timestep. ....	51
Figure 4.5 Pressure distribution convergence with iterations per timestep. ....	52
Figure 4.6 Pressure distribution convergence with iterations per timestep. ....	53
Figure 4.7 Cavity geometry convergence with panel discretization.....	54
Figure 4.8 Sensitivity of cavity geometry convergence to leading edge paneling. ....	55
Figure 4.9 Pressure distribution convergence with panel discretization.....	56
Figure 4.10 Convergence of cavity thickness growth with iterations per timestep. ....	57
Figure 4.11 Convergence of cavity thickness growth with iterations per timestep. ....	58
Figure 4.12 Comparison of Linear Cavity Shape and Non-Linear Cavity Shape .....	59
Figure 4.13 Comparison of Linear Theory and Non-Linear Theory for Pressure Distribution on the Pressure Side of a Flat Plate at $d/c = 1.0$ .....	60
Figure 4.14 Comparison of Linear and Non-Linear Theory for Pressure Distribution. ....	61
Figure 4.15 Comparison of Linear and Non-Linear Theory for Pressure Distribution. ....	62
Figure 4.16 Comparison of Linear and Non-Linear Theory for Pressure Distribution. ....	63





## List of Tables

Table 3.1: Panel Indexing for Entry Phase	31
Table 3.2: Panel indexing for Full Submergence	36
Table 4.1: CPU times for analysis of flat plate on a DEC Alphastation 600 5/266	56

# Chapter 1

## Introduction

### 1.1 Surface Piercing Hydrofoils and Propellers

During the 1970's surface piercing propellers were readily considered as an attractive means of propulsion for high speed surface crafts. Much of the pioneering theoretical work on the subject was done during this period. Surface piercing propellers, also called partially submerged propellers, are a class of propellers in which each blade is submerged for only a ratio (usually half) of a revolution, the shaft centerline being at the waterline. At each revolution the blade cuts the water surface, causing the flow to separate at both the leading edge of the suction side and at the trailing edge of the pressure side. This entrains an air filled cavity on the suction side of the blade, which vents to the atmosphere at the free surface. At high speed applications, these type of propellers, operating at low advance-coefficients, potentially provide higher efficiency than the alternative fully submerged propellers, be they fully wetted, partially cavitating or super-cavitating.

The improved performance is attributed to two major factors: (1) Reduction of hydrodynamic resistance from the appendages, including shafts, struts, propeller hubs, etc. The only surfaces that provide hydrodynamic resistance are the propeller blades and rudder. This last one can even be eliminated by using an articulated surface piercing drive system. (2) As opposed to cavitating propellers, the surface piercing propeller does not exhibit growing and collapsing cavities, which is a major source of vibration, blade surface erosion and acoustical noise. There is however still a major vibration issue due to the cyclical loading and unloading of the blades corresponding to the entering and exiting of the water surface.

In recent years, with the resurgence of increased demand for high speed vessels, surface piercing propellers have come back as an efficient alternative mode of propulsion. Hence the need for new improved robust and reliable numerical analysis tools such as the one presented in this work.

## **1.2 Previous Research**

The first recorded occurrence of the use of surface piercing propellers dates back to the late 1800's. Hadler and Hecker give a history overview in [4]. Up until the 1960's most of the surface piercing propeller design was based on empirical and experimental methods, since no theoretical basis existed for the performance analysis of such propulsor types.

### **1.2.1 Two-Dimensional Linear Theory**

The water entry and exit of a fully ventilated foil or thin wedge has been treated analytically by Yim [11] and Wang [9], using conformal mapping techniques. The blade geometry and the entrained cavity are considered to be thin, so that the linearization of the foil boundary and the boundary conditions are adopted. The speed of entry is considered fast enough, and the entire time duration is short enough, to allow using the infinite Froude number approximation for the free-surface boundary condition. In both author's work, the solution is divided in three phases: initial entry, complete entry, and exit phase.

Yim [11] included gravity effects in his solution. His results however showed that when the Froude number is larger than three, gravity effects on the force characteristics of the wedge are negligible. Yim also considers the flow to be symmetrical around the foil with respect to the axis of water entry. The cavity geometry is symmetric to the blade profile, with respect to the vertical axis of entry.

Wang [9] allowed the foil to have asymmetric blade and cavity profile, or essentially to have small time-dependent deformations. The pressure distribution on the foil is deter-

mined analytically up to a function of the time variable. Wang also considered oblique water entry and exit [10].

### **1.2.2 3-D Linearized Theory**

Furuya [3] developed a partially submerged propeller theory by employing a singularity distribution method. Unsteady pressure doublets and pressure sources represented the blade camber and blade-and-cavity thickness respectively. The induced velocities were derived by reducing the formula to a lifting line configuration. The free surface effect was considered by the image method.

Vorus [8] extended the methodology developed for calculating the forces on a fully submerged subcavitating propellers to surface piercing propellers. The derived analytical formulas are intended for the analysis of surface piercing propellers on high-performance planing crafts.

### **1.2.3 Experimental Work**

Cox [1] performed free-fall penetration tests for a two-dimensional thin, straight wedge at various speeds and wedge incidence angles.

Olofsson [7] did model experiments on partially submerged propellers destined for large commercial high speed vessels. He concluded that given the proper shaft yaw angle, very high efficiencies are possible. However, due to the dynamic loads, serious vibration and strength problems may arise.

## **1.3 Objectives of the Present Method**

The objective of this work is to develop a robust and computationally efficient nonlinear method for predicting the cavity shape and hydrodynamic forces on a surface piercing two-dimensional hydrofoil of arbitrary geometry. Even though the developed theory is two-dimensional, it is still very helpful for the design and analysis of surface piercing pro-

pellers. The flow over any section of the propeller is considered to be two-dimensional at any instant from entry of the blade in the water to its exit.

The presented theory is a nonlinear, time marching, potential based boundary element method. The cavity shape is found iteratively at each timestep of the hydrofoil trajectory through the fluid. Convergence studies and comparisons with linearized analytical methods are also shown in this work.

# Chapter 2

## Mathematical Formulation

### 2.1 Overview

In this chapter, the complete problem definition is laid out. Potential flow is assumed and Green's formula is applied on the exact blade and cavity surface. The complete boundary conditions on the foil surface, cavity and free surface are derived in detail, and the needed simplifications are justified. Next the derivation of the non-linear cavity geometry is shown. Finally the derivation of the unsteady pressure forces are provided.

### 2.2 Potential Flow and Green's Formula

One of the most robust and versatile panel methods currently in use, are based on perturbation potential theory. The flow is assumed to be incompressible, inviscid and irrotational. The governing equation everywhere inside the fluid region, is the continuity equation for conservation of mass, and is represented by Laplace's equation:

$$\nabla^2\Phi = 0 \tag{2.1}$$

In a fully unbounded fluid domain, without a free surface, the foil can be represented as shown in Figure 2.1.

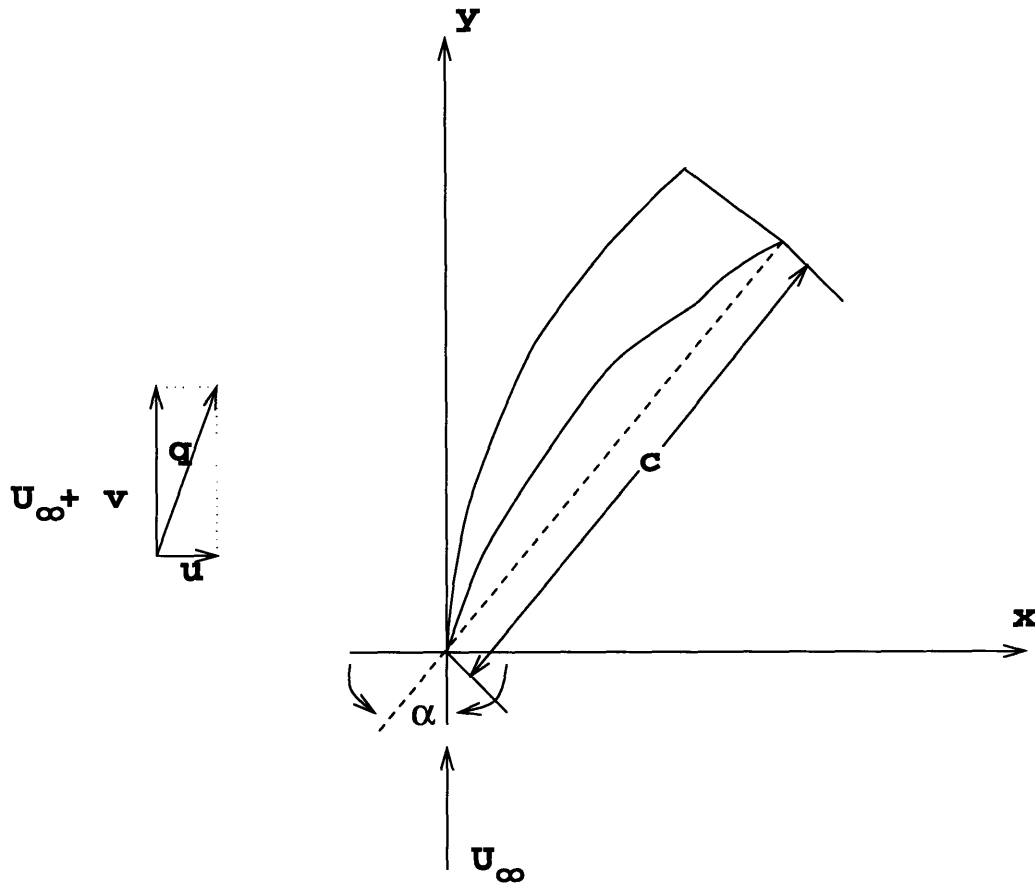


**Figure 2.1** Sketch of Hydrofoil in Unbounded Fluid.

The total velocity flow field,  $\vec{q}$ , can be expressed in terms of the total potential  $\Phi$ , or the perturbation potential,  $\phi$ , as:

$$\vec{q} = \nabla\Phi = U_{\infty} + \nabla\phi \quad (2.2)$$

$$\vec{q} = u\hat{i} + (U_{\infty} + v)\hat{j} \quad (2.3)$$

where  $\hat{i}$  and  $\hat{j}$  are the unit vectors in the horizontal and vertical axis respectively.

The total and perturbation potential are related by:

$$\phi(x, y) = \Phi(x, y) - \Phi_{in}(x, y) \quad (2.4)$$

where the inflow potential is defined by:

$$\Phi_{in}(x, y) = U_{\infty}y \quad (2.5)$$

The perturbation potential,  $\phi_p(x, y, t)$  at any point  $p$  which lies either on the wetted blade surface,  $S_{ws}(t)$ , or on the cavity surface,  $S_c(t)$ , is related to the perturbation potential and must satisfy Green's third identity:

$$\varepsilon\pi\phi_p = \int_{S_{ws}(t) \cup S_c(t)} \left[ \phi_q(t) \frac{\partial}{\partial n_q(t)} (G(p; q)) - G(p; q) \frac{\partial}{\partial n_q} \phi_q(t) \right] dS \quad (2.6)$$

where subscript  $q$  refers to the variable point in the integrations,  $n_q$  is the unit vector normal to the blade surface, or the cavity surface. The constant  $\varepsilon=1$  when the point  $p$  is on the wetted blade or cavity surface, otherwise it is equal to two. The Green's function  $G(p; q) = \ln[R(p; q)]$ , where  $R(p; q)$  is the distance from the field point  $p$  to the variable point  $q$ . Equation (2.1) expresses the perturbation potential on the surface formed by the blade and cavity surfaces, as a superposition of the potentials induced by a piecewise continuous source distribution  $G$ , and a piece wise continuous dipole distribution  $\partial G/\partial n$ .

Without the implementation of appropriate boundary conditions, the solution to equation (2.6) is not unique. The boundary conditions are explained separately in chapter 2.4 for a fully ventilated surface piercing hydrofoil.

### 2.3 Problem Definition

Consider a two-dimensional hydrofoil as shown in Figure 2.2, entering an air-water interface, which is initially at rest, with a constant velocity,  $U_{\infty}$ , normal to the free surface. The flow is considered with respect to the foil. The speed of entry is sufficiently high for



the foil to fully ventilate starting at the sharp leading edge and along the suction side. Ventilation can be treated as cavitation with the cavity pressure being equal to the atmospheric pressure at the free surface.

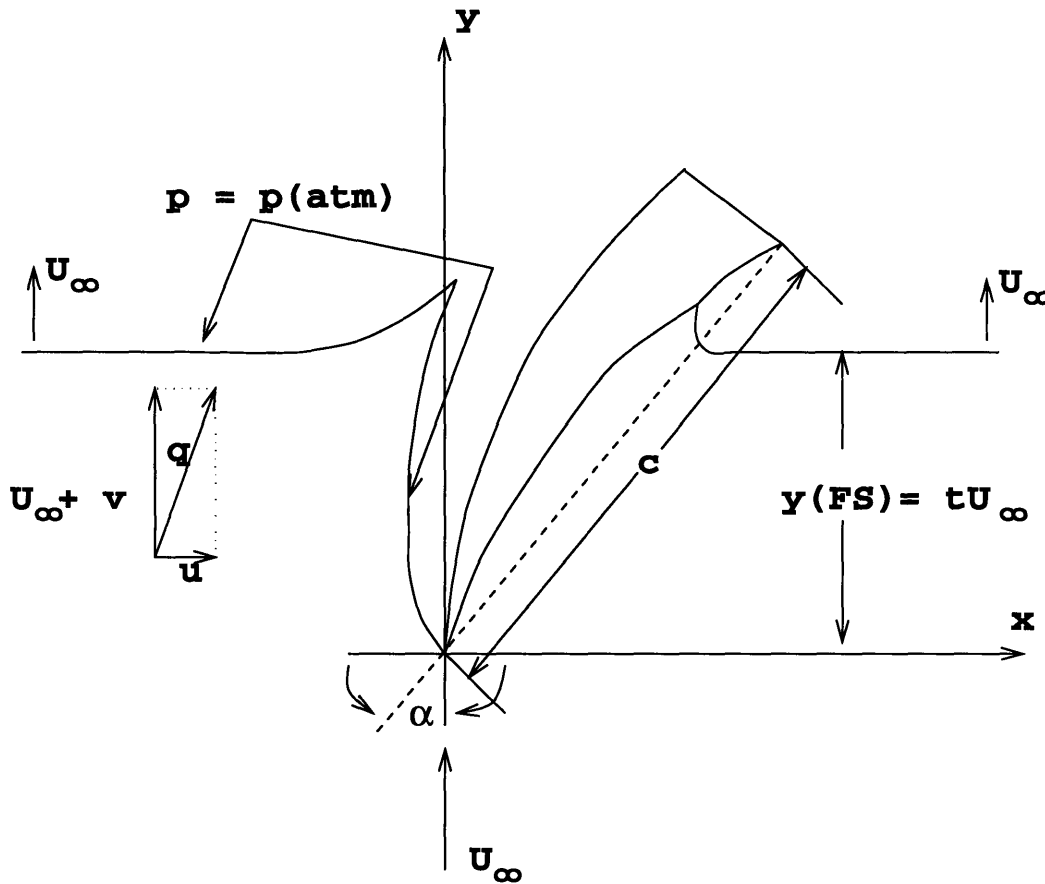


**Figure 2.2 :** Sketch of Surface Piercing Hydrofoil with Coordinate System Moving with the Foil

## 2.4 Boundary Conditions

### 2.4.1 Free Surface Boundary Conditions

The Froude number is defined as (2.7) for hydrofoils, and as (2.8) for propellers

$$F_r = \frac{U_\infty}{\sqrt{gc}} \tag{2.7}$$

$$F_r = \frac{U_\infty}{\sqrt{gD}} \quad (2.8)$$

where  $g$  is the gravitational constant,  $c$  is the foil chord length, and  $D$  is the propeller diameter. Throughout this work, an infinite Froude number may be assumed as a valid simplification. This assumption is valid since optimum applications of cavitating hydrofoils and propellers, usually operate at high speeds. For example a hydrofoil born vessel operating at 50 knots and having a foil chord length of 0.5m will have a Froude number of about 11. A full scale surface piercing propeller with a diameter of 0.75m operating on a ship advancing at 40 knots, gives a Froude number of about 7.6. Yim [11] concluded that gravity effects are negligible for Froude numbers larger than 3. Thus for applications where surface piercing hydrofoils or propellers are efficient, the Froude number defined by equation (2.7) is in the 5-10 range.

Applying Bernoulli's equation on the free surface gives the dynamic boundary condition there:

$$-\left(\frac{p - p_{atm}}{\rho}\right) = \frac{\partial\phi}{\partial t} + \frac{1}{2}\left(\dot{q} \cdot \dot{q} - U_\infty^2\right) + g\eta = 0 \quad (2.9)$$

where  $\eta$ , is the free surface elevation.

Leaving out higher order terms to linearize the above equation and rewriting (2.9) in steady state form, we obtain:

$$U_\infty \frac{\partial\phi}{\partial x} + g\eta = 0 \quad (2.10)$$

By introducing the following non-dimensionalizations:

$$\eta' = \frac{\eta}{c} ; x' = \frac{x}{c} ; \phi' = \frac{\phi}{U_{\infty} c} \quad (2.11)$$

we get:

$$\frac{\partial}{\partial x'} \phi' + \frac{\eta'}{F_r^2} = 0 \quad (2.12)$$

Since we assumed infinite Froude number, the linear dynamic boundary condition on the free surface is reduced to zero horizontal perturbation velocity.

$$\frac{\partial \phi}{\partial x} = u = 0 \quad (2.13)$$

#### 2.4.2 Dynamic and Kinematic Foil Boundary Conditions

The flow is required to be tangential to the wetted hydrofoil surface, as well as to the cavity surface. The kinematic boundary condition is given by:

$$\frac{\partial \phi}{\partial n} = -U_{\infty} \cdot \hat{n} \quad (2.14)$$

where  $n$  is the unit normal to the hydrofoil or cavity surface, directed into the fluid domain. This condition is applied to the exact non-linear cavity surface and wetted foil surface.

The perturbation potential on the cavity will be a function of submergence and time, and will be convected with the flow. In linear theory [9] [11], this is equivalent to having the perturbation potential as a function of  $(U_{\infty} t - y)$  only.

To find the cavity shape at subsequent iterations, the cavity surface is convected with the local velocity. Henceforth, this condition is non-linear in nature. This is somewhat analogous to that of the shed vorticity in the wake of an oscillating foil or a foil in unsteady inflow.

Finally, at the leading edge, continuity of perturbation potential must be satisfied:

$$\phi_{wetted}|_{LE} = \phi_{cavity}|_{LE} \quad (2.15)$$

Similarly when the foil is fully submerged and a ventilated cavity starts to grow at the trailing edge of the wetted part of the foil, continuity of perturbation potential must also be satisfied there:

$$\phi_{wetted}|_{TE} = \phi_{cavity}|_{TE} \quad (2.16)$$

## 2.5 Non-Linear Cavity Shape Determination

The cavity shape is found iteratively by aligning the panels so that the flow is tangent to the cavity surface (2.14). Before convergence, the flow along the cavity surface consists of the vector summation of the velocities shown in Figure 2.3

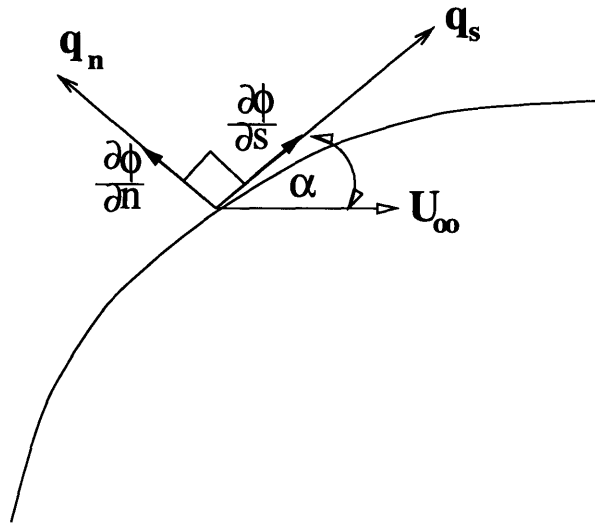


**Figure 2.3** Vector diagram of cavity surface velocities before convergence

where

$$q_s = \frac{\partial \phi}{\partial s} + U_\infty \cos(\alpha) \quad (2.17)$$

$$q_n = \frac{\partial \phi}{\partial n} - U_\infty \sin(\alpha)$$

The update of the cavity surface position,  $h$ , needs to be iteratively modified such that the flow is tangential to the surface. A complete derivation of this condition is made by Kinnas and Fine in [5].

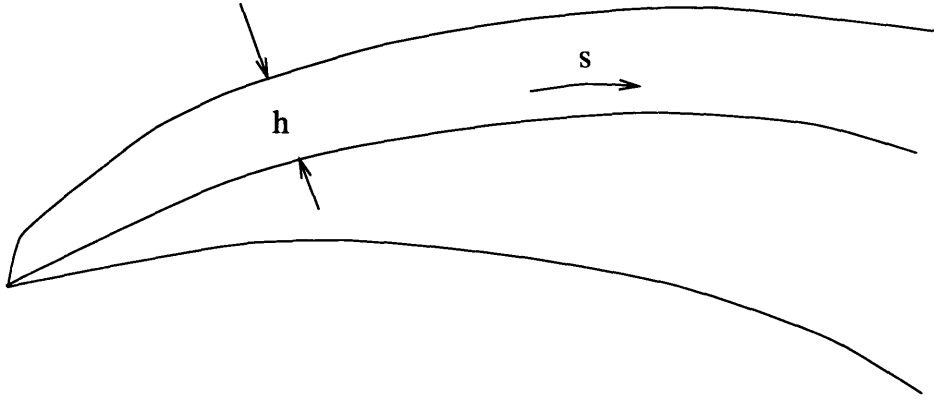


**Figure 2.4** Sketch of cavity surface height update at each iteration

Making use of the above velocity vector diagram, the cavity surface update is shown to be equivalent to:

$$\left[ \frac{\partial \phi}{\partial s} + U_{\infty} \cos(\alpha) \right] \frac{\partial h}{\partial s} = \frac{\partial \phi}{\partial n} - U_{\infty} \sin(\alpha) \quad (2.18)$$

Finally, making use of equation (2.17), the change in cavity height is reduced to:

$$\frac{\partial h}{\partial s} = \frac{q_n}{q_s} \quad (2.19)$$

At each timestep of the foil entry, the cavity shape is found iteratively, until the change in cavity height is zero.

## 2.6 Pressures on the Foil and Cavity Surface

Consider the flow with respect to the moving foil as shown in Figure 2.2. After the initial entry, the flow at infinity and the free-surface move with speed  $U_\infty$ . The unsteady Bernoulli equation will be:

$$p + \rho \frac{\partial \phi}{\partial t} + \frac{\rho}{2} \dot{q}^2 + \rho g y = C(t) \quad (2.20)$$

where  $p$  is the pressure in the fluid domain,  $\rho$  is the density. The constant  $C(t)$  can be found by applying equation (2.20) at a point on the free surface, far from the intersection with the foil and cavity.

$$C(t) = p_{atm} + \frac{\rho}{2} U_\infty^2 + \rho g y_{FS} \quad (2.21)$$

where  $y_{FS}$  is the  $y$  location of the free surface.

$$y_{FS} = U_\infty \cdot t \quad (2.22)$$

Introducing the following non-dimensional quantities:

$$t' = t \frac{U_\infty}{c} ; y' = \frac{y}{c} ; \phi' = \frac{\phi}{U_\infty c} \quad (2.23)$$

we finally obtain

$$\frac{p}{U_\infty^2} + \rho \frac{\partial}{\partial t'} \phi' + \frac{\rho}{2} \frac{\dot{q}^2}{U_\infty^2} + \frac{\rho y'}{F_r^2} = \frac{p_{atm}}{U_\infty^2} + \frac{\rho}{2} + \frac{\rho t'}{F_r^2} \quad (2.24)$$

where we also substituted for the Froude number. Being consistent with our infinite Froude number assumption, the hydrostatic terms in equations (2.20) and (2.21) drop out.

So finally, the pressure equation to be applied, at any point B, on the fully wetted part of the foil and cavity surface is:

$$C_p = \frac{p_B - p_{atm}}{\frac{\rho}{2} U_\infty^2} = 1 - \left( \frac{q_B}{U_\infty} \right)^2 - 2 \frac{\partial \phi_B}{\partial t} \frac{1}{U_\infty^2} \quad (2.25)$$

Notice that  $p_B$  must be equal to  $p_{atm}$  on the free surface, as well as inside the cavity, since it is ventilated to the free surface. Since the perturbation potential on the cavity surfaces is convected with the flow, we expect the pressure coefficient to be equal to zero. This will be investigated and confirmed in the numerical implementation.





# Chapter 3

## Discrete Formulation

### 3.1 Discretized Surface Piercing Foil Geometry

The trajectory of the surface piercing foil can be subdivided in four geometric stages. The first stage is when only part of the foil chord length is submerged below the free surface, as shown in Figure 3.1. This is the most important phase from the hydrodynamic point of view, as the pressure loads and hydrodynamic forces undergo the greatest changes.

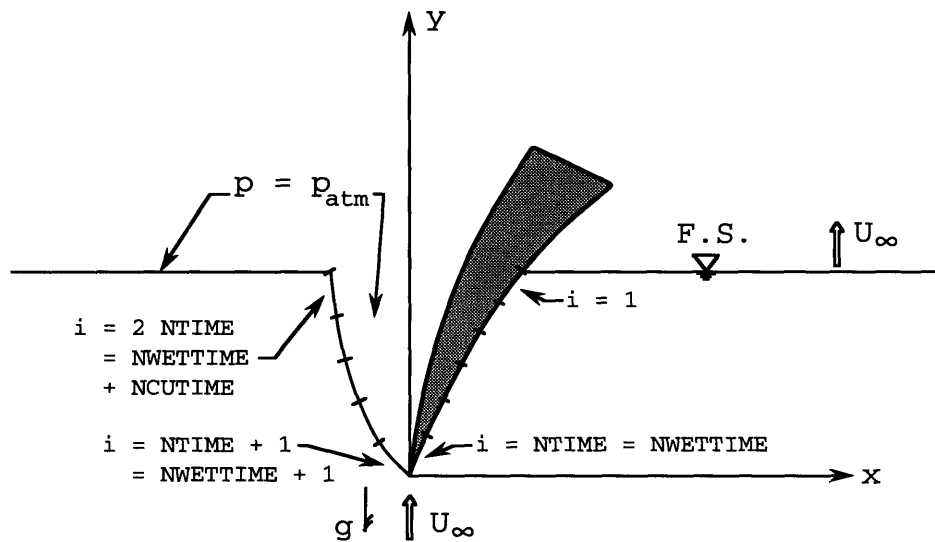


**Figure 3.1** Discretized foil and cavity geometry. Panel indexing of foil and cavity for partially submerged chord length

At the end of this stage the trailing edge of the foil is at the free surface as shown in Figure 3.2. The panel indexing and numbering are shown in Table 3.1.

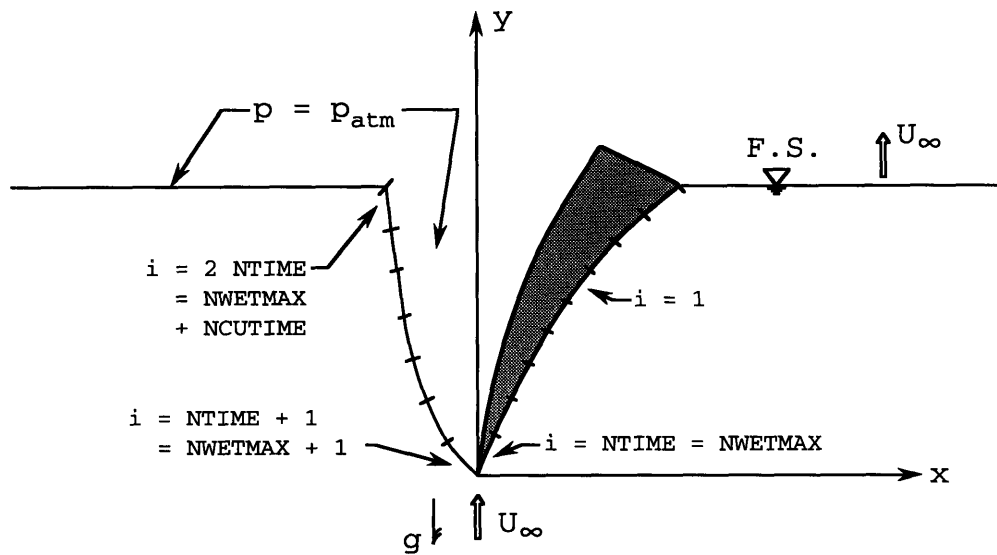


**Figure 3.2** Discretized foil and cavity geometry. Panel indexing of foil and cavity for full chord submergence

After further entry, a ventilated cavity is shed aft of the trailing edge of the pressure side of the foil as shown in Figure 3.3. The last timestep of this stage, corresponds to the equivalent distance travelled by a surface piercing blade section, and is shown in Figure 3.4. The panel indexing and numbering for these last two phases are shown in Table 3.2.

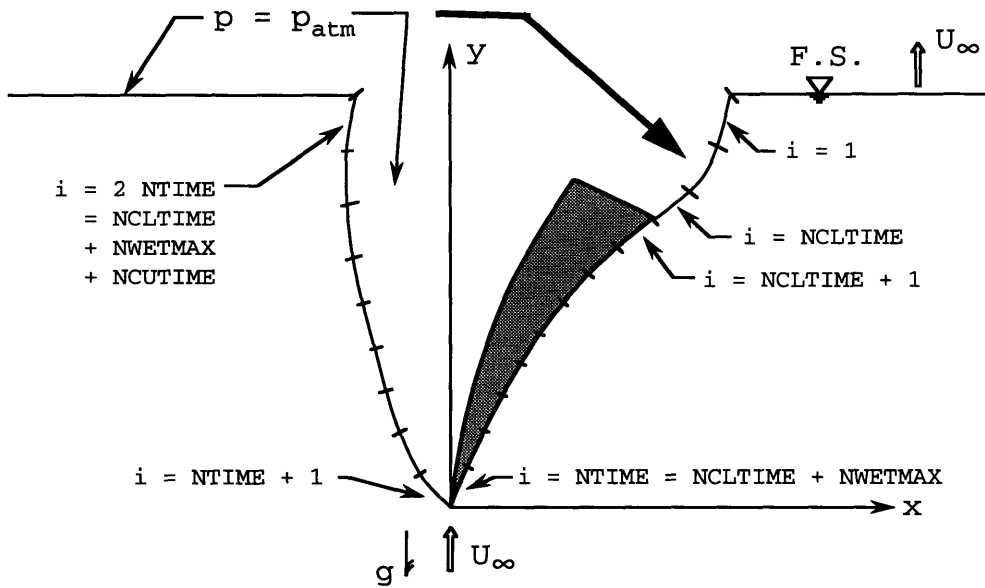


**Figure 3.3** Discretized foil and cavity geometry. Panel indexing of foil and cavity for fully submerged stage.

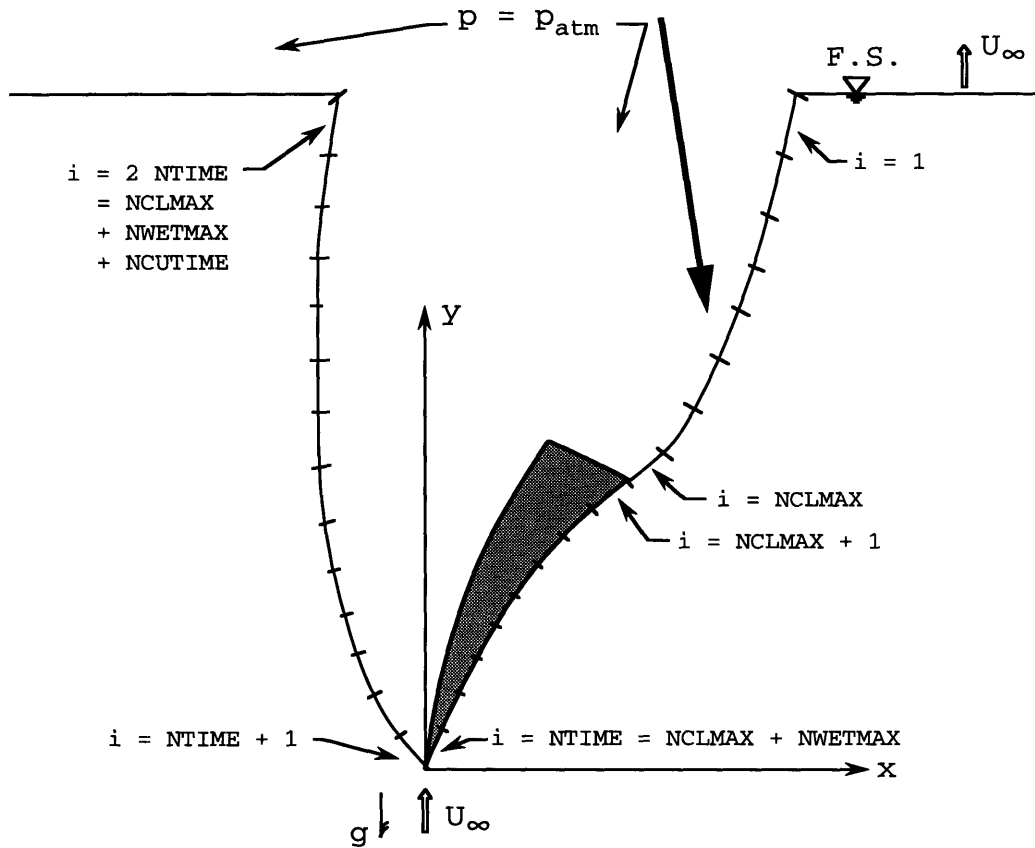


**Figure 3.4** Discretized foil and cavity geometry. Panel indexing of foil and cavity at *end* of fully submerged stage

### 3.2 Discretized Green's Formula

The discretized form of Green's theorem is applied to each panel on the actual foil and cavity surface:

$$\pi\phi_i = \sum_j S_{ij} \frac{\partial\phi_j}{\partial n} - \sum_j D_{ij} \phi_j \quad (3.1)$$

where  $S_{ij}$  and  $D_{ij}$  are the influence coefficients due to a source of uniform unit strength and a normal dipole of uniform unit strength respectively. These include the effects of the free surface images, which are discussed in more detail in the next chapter.

In matrix form, the system of equations to be solved becomes:

$$\begin{bmatrix} D_{11} & \dots & \dots & \dots & \dots & D_{1j} \\ \dots & \dots & \dots & \dots & \dots & \dots \\ \dots & \dots & \dots & \dots & \dots & \dots \\ \dots & \dots & \dots & \dots & \dots & \dots \\ \dots & \dots & \dots & \dots & \dots & \dots \\ D_{i1} & \dots & \dots & \dots & \dots & D_{ij} \end{bmatrix} \begin{bmatrix} \phi_1 \\ \dots \\ \dots \\ \dots \\ \dots \\ \phi_j \end{bmatrix} = \begin{bmatrix} S_{11} & \dots & \dots & \dots & \dots & S_{1j} \\ \dots & \dots & \dots & \dots & \dots & \dots \\ \dots & \dots & \dots & \dots & \dots & \dots \\ \dots & \dots & \dots & \dots & \dots & \dots \\ \dots & \dots & \dots & \dots & \dots & \dots \\ S_{i1} & \dots & \dots & \dots & \dots & S_{ij} \end{bmatrix} \begin{bmatrix} \frac{\partial \phi_1}{\partial n} \\ \dots \\ \dots \\ \dots \\ \dots \\ \frac{\partial \phi_j}{\partial n} \end{bmatrix} \quad (3.2)$$

### 3.3 Free Surface Boundary Condition

The method of “negative imaging”, is used to enforce the free surface boundary condition (2.13). The imaged foil and cavity, shown in Figure 3.5, is represented by sinks and dipoles with opposite normal. As mentioned in the previous chapter, the influence coefficients include the effects of the free surface image as follows:

$$D_{ij} = \left[ \int_{S_{ws,c|_j}} \frac{\partial}{\partial n} (\ln R) ds \right]_{\text{submerged part}} - \left[ \int_{S_{ws,c|_j}} \frac{\partial}{\partial n} (\ln R) ds \right]_{\text{imaged part}} \quad (3.3)$$

$$S_{ij} = \left[ \int_{S_{ws,c|_j}} (\ln R) ds \right]_{\text{submerged part}} - \left[ \int_{S_{ws,c|_j}} (\ln R) ds \right]_{\text{imaged part}} \quad (3.4)$$

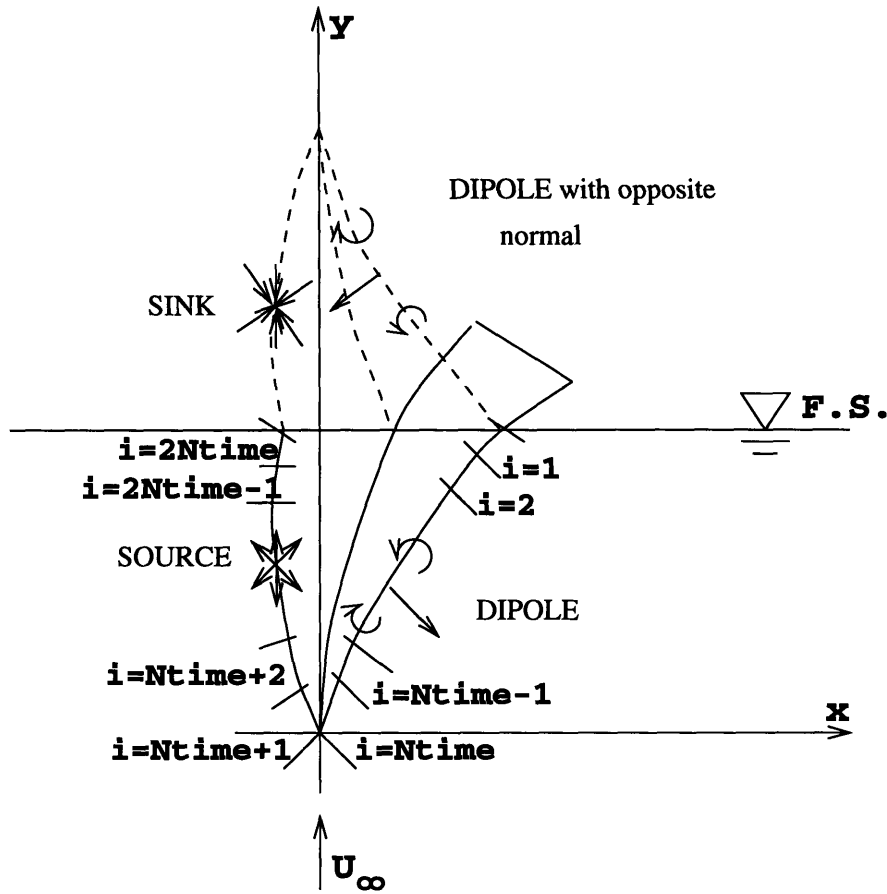


**Figure 3.5** Perturbation Potential Distribution on Actual Foil and Cavity surface and Their Images

### 3.4 Governing System of Equations

Re-arranging (3.2) for the unknown quantities, dipole strength on the wetted surface and source strength on the cavity in the left hand side and the known quantities, source strength on the wetted surface and dipole strength on the cavity in the right hand side, we obtain the following system of equations:

$$[A] [x] = [B] [y] \tag{3.5}$$

where [A] and [B] are the influence coefficient matrices, [x] in the vector of unknown and [y] is the vector of known values. The matrices [A] and [B] are square and full. At any timestep NTIME, the [A] and [B] matrices are of size (2 NTIME)\*(2 NTIME), and the vectors [x] and [y] are of size (2 NTIME).

In a modular fashion the above equation (3.5) can be expanded as:

$$\begin{aligned}
 & \begin{bmatrix} [S]_{CL} & [D]_{WET} & [S]_{CU} \end{bmatrix} \begin{bmatrix} -\left[\frac{\partial\phi}{\partial n}\right]_{CL} \\ [\phi]_{WET} \\ -\left[\frac{\partial\phi}{\partial n}\right]_{CU} \end{bmatrix} \\
 & = \begin{bmatrix} [D]_{CL} & [S]_{WET} & [D]_{CU} \end{bmatrix} \begin{bmatrix} -[\phi]_{CL} \\ \left[\frac{\partial\phi}{\partial n}\right]_{WET} \\ -[\phi]_{CU} \end{bmatrix}
 \end{aligned} \tag{3.6}$$

where [S] and [D] are the influence coefficient matrices due to a source of uniform strength and dipole of uniform strength respectively. The subscripts CL, WET, and CU refer to the “lower” cavity, or pressure side panels, wetted foil panels and “upper” cavity, or suction side panels respectively.

### 3.4.1 Phase I: Initial Entry

During Phase 1, the entry problem, the foil starts to cut through the free surface, as seen in Figure 3.1, until the entire chord length is submerged, i.e. foil trailing edge panel is as the free surface, as shown in Figure 3.2. During this phase there is no lower cavity surface yet, so the corresponding governing system of equations is similar to the one above, but without the [S] and [D] matrices corresponding to the lower cavity surface, as well as the omission of the  $\left[\frac{\partial\phi}{\partial n}\right]$  vector corresponding to the lower cavity surface.



We can thus rewrite the system of equations (3.6) as:

$$\begin{aligned}
 & \begin{bmatrix} [D]_{WET} & [S]_{CU} \end{bmatrix} \begin{bmatrix} [\phi]_{WET} \\ -\left[\frac{\partial\phi}{\partial n}\right]_{CU} \end{bmatrix} \\
 & = \begin{bmatrix} [S]_{WET} & [D]_{CU} \end{bmatrix} \begin{bmatrix} \left[\frac{\partial\phi}{\partial n}\right]_{WET} \\ -[\phi]_{CU} \end{bmatrix}
 \end{aligned} \tag{3.7}$$

At any timestep NTIME the panel indexing is given in Table 3.1:

**Table 3.1 : Panel Indexing for Entry Phase**

	Modular Indexing	Global Indexing	Note
At Timestep NTIME			
Wetted Surface	TE = 1 LE = NWETTIME	TE = 1 LE = NTIME	
Cavity Surface	LE = 1 TE = NCUTIME	LE = NTIME+1 TE = 2 * NTIME	NCUTIME = NWETTIME
At Full Submergence			
Wetted Surface	TE = 1 LE = NWETMAX	TE = 1 LE = NWETMAX	
Cavity Surface	LE = 1 TE = NCUMAX	LE = NWETMAX+1 TE = NWEMAX+ NCUMAX	NCUMAX = NWETMAX

At any timestep Ntime the left hand side of the governing system of equations can be represented by each module as follows:

$$\begin{aligned}
[D]_{WET} &= \begin{bmatrix} D_{1,1} & \cdots & D_{1,Ntime} \\ \cdots & \cdots & \cdots \\ D_{Ntime,1} & \cdots & D_{Ntime,Ntime} \\ D_{Ntime+1,1} & \cdots & D_{Ntime+1,Ntime} \\ \cdots & \cdots & \cdots \\ D_{2Ntime,1} & \cdots & D_{2Ntime,Ntime} \end{bmatrix} \\
[S]_{CU} &= \begin{bmatrix} S_{1,Ntime+1} & \cdots & S_{1,2Ntime} \\ \cdots & \cdots & \cdots \\ S_{Ntime,Ntime+1} & \cdots & S_{Ntime,2Ntime} \\ S_{Ntime+1,Ntime+1} & \cdots & S_{Ntime+1,2Ntime} \\ \cdots & \cdots & \cdots \\ S_{2Ntime,Ntime+1} & \cdots & S_{2Ntime,2Ntime} \end{bmatrix}
\end{aligned} \tag{3.8}$$

$$[\phi]_{WET} = \begin{bmatrix} \phi_1 \\ \cdots \\ \phi_{Ntime} \end{bmatrix} ; \quad \left[ \frac{\partial \phi}{\partial n} \right]_{CU} = \begin{bmatrix} \frac{\partial \phi_{Ntime+1}}{\partial n} \\ \cdots \\ \frac{\partial \phi_{2Ntime}}{\partial n} \end{bmatrix} \tag{3.9}$$

At any timestep  $Ntime$  the right hand side of the governing system of equations can be represented by each module as follows:

$$\begin{aligned}
[S]_{WET} &= \begin{bmatrix} S_{1,1} & \cdots & S_{1,Ntime} \\ \cdots & \cdots & \cdots \\ S_{Ntime,1} & \cdots & S_{Ntime,Ntime} \\ S_{Ntime+1,1} & \cdots & S_{Ntime+1,Ntime} \\ \cdots & \cdots & \cdots \\ S_{2Ntime,1} & \cdots & S_{2Ntime,Ntime} \end{bmatrix} \\
[D]_{CU} &= \begin{bmatrix} D_{1,Ntime+1} & \cdots & D_{1,2Ntime} \\ \cdots & \cdots & \cdots \\ D_{Ntime,Ntime+1} & \cdots & D_{Ntime,2Ntime} \\ D_{Ntime+1,Ntime+1} & \cdots & D_{Ntime+1,2Ntime} \\ \cdots & \cdots & \cdots \\ D_{2Ntime,Ntime+1} & \cdots & D_{2Ntime,2Ntime} \end{bmatrix}
\end{aligned} \tag{3.10}$$

$$\left[ \frac{\partial \phi}{\partial n} \right]_{WET} = \begin{bmatrix} \frac{\partial \phi_1}{\partial n} \\ \dots \\ \frac{\partial \phi_{Ntime}}{\partial n} \end{bmatrix} ; [\phi]_{CU} = \begin{bmatrix} \phi_{Ntime+1} \\ \dots \\ \phi_{2Ntime} \end{bmatrix} \quad (3.11)$$

From continuity of perturbation potential at the leading edge of the foil, (2.15) takes the discretized form of:

$$\phi_{Ntime+1} = \phi_{Ntime} \quad (3.12)$$

Strictly speaking, the perturbation potential on the wetted side and the cavity side are only equal at the exact leading edge point, and not at the control points of the panels as indicated in (3.12). A more accurate way of representing the leading edge continuity of perturbation potential is to make use the y-location of the control points of the leading edge panels for the linear interpolation:

$$\phi_{Ntime+1} = \phi_{Ntime} \frac{y_{Ntime}}{y_{Ntime+1}} \quad (3.13)$$

Making use of this continuity and assembling all the above modules, we obtain:

$$\begin{bmatrix}
D_{1,1} & \dots & K_1 & S_{1,Ntime+1} & \dots & S_{1,2Ntime} \\
\dots & \dots & \dots & \dots & \dots & \dots \\
D_{Ntime,1} & \dots & K_{Ntime} & S_{Ntime,Ntime+1} & \dots & S_{Ntime,2Ntime} \\
D_{Ntime+1,1} & \dots & K_{Ntime+1} & S_{Ntime+1,Ntime+1} & \dots & S_{Ntime+1,2Ntime} \\
\dots & \dots & \dots & \dots & \dots & \dots \\
D_{2Ntime,1} & \dots & K_{2Ntime} & S_{2Ntime,Ntime+1} & \dots & S_{2Ntime,2Ntime}
\end{bmatrix}
\begin{bmatrix}
\phi_1 \\
\dots \\
\phi_{Ntime} \\
-\left(\frac{\partial \phi_{Ntime+1}}{\partial n}\right) \\
\dots \\
-\left(\frac{\partial \phi_{2Ntime}}{\partial n}\right)
\end{bmatrix} = \quad (3.14)$$

$$\begin{bmatrix}
S_{1,1} & \dots & S_{1,Ntime} & D_{1,Ntime+1} & \dots & D_{1,2Ntime} \\
\dots & \dots & \dots & \dots & \dots & \dots \\
S_{Ntime,1} & \dots & S_{Ntime,Ntime} & D_{Ntime,Ntime+1} & \dots & D_{Ntime,2Ntime} \\
S_{Ntime+1,1} & \dots & S_{Ntime+1,Ntime} & D_{Ntime+1,Ntime+1} & \dots & D_{Ntime+1,2Ntime} \\
S_{Ntime+2,1} & \dots & S_{Ntime+2,Ntime} & D_{Ntime+2,Ntime+1} & \dots & D_{Ntime+2,2Ntime} \\
\dots & \dots & \dots & \dots & \dots & \dots \\
S_{2Ntime,1} & \dots & S_{2Ntime,Ntime} & D_{2Ntime,Ntime+1} & \dots & D_{2Ntime,2Ntime}
\end{bmatrix}
\begin{bmatrix}
\frac{\partial \phi_1}{\partial n} \\
\dots \\
\frac{\partial \phi_{Ntime}}{\partial n} \\
0 \\
-(\phi_{Ntime+2}) \\
\dots \\
-(\phi_{2Ntime})
\end{bmatrix}$$

Notice that the Ntime+1 element in the right hand side vector is zero: perturbation potential on cavity leading edge panel is equal to the perturbation potential on wetted leading edge panel), and hence the following substitution in the column Ntime of the left hand side matrix:

$$K_i = D_{1,Ntime} + D_{i,Ntime+1} \left( \frac{y_{Ntime}}{y_{Ntime+1}} \right) ; \quad i=1 \dots 2Ntime \quad (3.15)$$

Where  $y_{Ntime+1}$  is the y-location of the leading edge cavity panel control point and  $y_{Ntime}$  is the y-location of the leading edge wetted panel control point.

But now, since the perturbation potentials on the cavity, at time Ntime, are known from the previous timesteps in the following manner:

$$\begin{aligned}\phi_j|_{t= Ntime} &= \phi_{LE}|_{t=i} ; j = Ntime + 2 \dots 2Ntime ; i = Ntime - 1 \dots 1 \\ \phi_j|_{t= Ntime} &= 0 ; j = Ntime + 1\end{aligned}\quad (3.16)$$

this can then be substituted into (3.14) and we finally obtain the fully discretized system of equations to be solved any time  $T=Ntime.\Delta t$ , and where  $T=0$  at the moment the foil enters the free surface.

$$\begin{bmatrix} D_{1,1} & \dots & K_1 & S_{1,Ntime+1} & \dots & S_{1,2Ntime} \\ \dots & \dots & \dots & \dots & \dots & \dots \\ D_{Ntime,1} & \dots & K_{Ntime} & S_{Ntime,Ntime+1} & \dots & S_{Ntime,2Ntime} \\ D_{Ntime+1,1} & \dots & K_{Ntime+1} & S_{Ntime+1,Ntime+1} & \dots & S_{Ntime+1,2Ntime} \\ \dots & \dots & \dots & \dots & \dots & \dots \\ D_{2Ntime,1} & \dots & K_{2Ntime} & S_{2Ntime,Ntime+1} & \dots & S_{2Ntime,2Ntime} \end{bmatrix} \begin{bmatrix} \phi_1 \\ \dots \\ \phi_{Ntime} \\ -\left(\frac{\partial \phi}{\partial n}\right)_{Ntime+1} \\ \dots \\ -\left(\frac{\partial \phi}{\partial n}\right)_{2Ntime} \end{bmatrix} = \quad (3.17)$$

$$\begin{bmatrix} S_{1,1} & \dots & S_{1,Ntime} & D_{1,Ntime+1} & \dots & D_{1,2Ntime} \\ \dots & \dots & \dots & \dots & \dots & \dots \\ S_{Ntime,1} & \dots & S_{Ntime,Ntime} & D_{Ntime,Ntime+1} & \dots & D_{Ntime,2Ntime} \\ S_{Ntime+1,1} & \dots & S_{Ntime+1,Ntime} & D_{Ntime+1,Ntime+1} & \dots & D_{Ntime+1,2Ntime} \\ S_{Ntime+2,1} & \dots & S_{Ntime+2,Ntime} & D_{Ntime+2,Ntime+1} & \dots & D_{Ntime+2,2Ntime} \\ \dots & \dots & \dots & \dots & \dots & \dots \\ S_{2Ntime,1} & \dots & S_{2Ntime,Ntime} & D_{2Ntime,Ntime+1} & \dots & D_{2Ntime,2Ntime} \end{bmatrix} \begin{bmatrix} \frac{\partial \phi}{\partial n} \\ \dots \\ \frac{\partial \phi}{\partial n} \\ 0 \\ -\phi_{LE}|_{t=Ntime-1} \\ \dots \\ -\phi_{LE}|_{t=1} \end{bmatrix}$$

### 3.4.2 Phase II, Complete Submergence

During phase 2, the fully submerged problem, the foil is entirely below the free surface and a ventilated cavity has started growing along the trailing edge of the lower side of the foil, as shown in Figure 3.3 and Figure 3.4.

We can thus rewrite the system of equations as:

$$\begin{aligned}
& \begin{bmatrix} [S]_{CL} & [D]_{WET} & [S]_{CU} \end{bmatrix} \begin{bmatrix} -\left[\frac{\partial\phi}{\partial n}\right]_{CL} \\ [\phi]_{WET} \\ -\left[\frac{\partial\phi}{\partial n}\right]_{CU} \end{bmatrix} \\
& = \begin{bmatrix} [D]_{CL} & [S]_{WET} & [D]_{CU} \end{bmatrix} \begin{bmatrix} -[\phi]_{CL} \\ \left[\frac{\partial\phi}{\partial n}\right]_{WET} \\ -[\phi]_{CU} \end{bmatrix}
\end{aligned} \tag{3.18}$$

At any timestep NTIME the panel indexing is given in Table 3.2:

**Table 3.2 : Panel Indexing for Full Submergence**

	Modular Indexing	Global Indexing	Note
<b>At Timestep NTIME</b>			
Lower Cavity Surface	FS = 1 TE = NCLTIME	FS = 1 TE = NTIME - NWETMAX	
Wetted Surface	TE = 1 LE = NWETTIME	TE=NTIME - NWETMAX+ 1 LE = NTIME	NWETTIME= NWETMAX
Upper Cavity Surface	LE = 1 TE = NCUTIME	LE = NTIME + 1 TE= 2*NTIME	NCUTIME = NCLTIME + NWETMAX
<b>At Full Submergence (just before exit phase)</b>			
Lower Cavity Surface	FS = 1 TE = NCLMAX	FS = 1 TE = NCLMAX	
Wetted Surface	TE = 1 LE = NWETMAX	TE = NCLMAX + 1 LE = NCLMAX + NWETMAX	

**Table 3.2 : Panel Indexing for Full Submergence**

	Modular Indexing	Global Indexing	Note
Cavity Surface	LE = 1 TE = NCUMAX	LE = NCLMAX + NWETMAX + 1 TE = NCLMAX + NWETMAX + NCUMAX	NCUMAX = NCLMAX + NWETMAX

At any timestep Ntime the left hand side of the governing system of equations can be represented by each module as follows:

$$[S]_{CL} = \begin{bmatrix} S_{1,1} & \cdots & S_{1,Ntime-Nwetmax} \\ \cdots & \cdots & \cdots \\ S_{Ntime,1} & \cdots & S_{Ntime,Ntime-Nwetmax} \\ S_{Ntime+1,1} & \cdots & S_{Ntime+1,Ntime-Nwetmax} \\ \cdots & \cdots & \cdots \\ S_{2Ntime,1} & \cdots & S_{2Ntime,Ntime-Nwetmax} \end{bmatrix} \quad (3.19)$$

$$[D]_{WET} = \begin{bmatrix} D_{1,Ntime-Nwetmax+1} & \cdots & D_{1,Ntime} \\ \cdots & \cdots & \cdots \\ D_{Ntime,Ntime-Nwetmax+1} & \cdots & D_{Ntime,Ntime} \\ D_{Ntime+1,Ntime-Nwetmax+1} & \cdots & D_{Ntime+1,Ntime} \\ \cdots & \cdots & \cdots \\ D_{2Ntime,Ntime-Nwetmax+1} & \cdots & D_{2Ntime,Ntime} \end{bmatrix}$$

$$[S]_{CU} = \begin{bmatrix} S_{1,Ntime+1} & \cdots & S_{1,2Ntime} \\ \cdots & \cdots & \cdots \\ S_{Ntime,Ntime+1} & \cdots & S_{Ntime,2Ntime} \\ S_{Ntime+1,Ntime+1} & \cdots & S_{Ntime+1,2Ntime} \\ \cdots & \cdots & \cdots \\ S_{2Ntime,Ntime+1} & \cdots & S_{2Ntime,2Ntime} \end{bmatrix}$$

$$\left[ \frac{\partial \phi}{\partial n} \right]_{CL} = \begin{bmatrix} \frac{\partial \phi_1}{\partial n} \\ \cdots \\ \frac{\partial \phi_{N1}}{\partial n} \end{bmatrix} ; [\phi]_{WET} = \begin{bmatrix} \phi_{N1+1} \\ \cdots \\ \phi_{Ntime} \end{bmatrix} ; \left[ \frac{\partial \phi}{\partial n} \right]_{CU} = \begin{bmatrix} \frac{\partial \phi_{Ntime+1}}{\partial n} \\ \cdots \\ \frac{\partial \phi_{2Ntime}}{\partial n} \end{bmatrix} \quad (3.20)$$

At any timestep  $N_{time}$  the right hand side of the governing system of equations can be represented by each module as follows:

$$\begin{aligned}
 [D]_{CL} &= \begin{bmatrix} D_{1,1} & \cdots & D_{1,N_{time}-N_{wetmax}} \\ \cdots & \cdots & \cdots \\ D_{N_{time},1} & \cdots & D_{N_{time},N_{time}-N_{wetmax}} \\ D_{N_{time}+1,1} & \cdots & D_{N_{time}+1,N_{time}-N_{wetmax}} \\ \cdots & \cdots & \cdots \\ D_{2N_{time},1} & \cdots & D_{2N_{time},N_{time}-N_{wetmax}} \end{bmatrix} \\
 [S]_{WET} &= \begin{bmatrix} S_{1,N_{time}-N_{wetmax}+1} & \cdots & S_{1,N_{time}} \\ \cdots & \cdots & \cdots \\ S_{N_{time},N_{time}-N_{wetmax}+1} & \cdots & S_{N_{time},N_{time}} \\ S_{N_{time}+1,N_{time}-N_{wetmax}+1} & \cdots & S_{N_{time}+1,N_{time}} \\ \cdots & \cdots & \cdots \\ S_{2N_{time},N_{time}-N_{wetmax}+1} & \cdots & S_{2N_{time},N_{time}} \end{bmatrix} \\
 [D]_{CU} &= \begin{bmatrix} D_{1,N_{time}+1} & \cdots & D_{1,2N_{time}} \\ \cdots & \cdots & \cdots \\ D_{N_{time},N_{time}+1} & \cdots & D_{N_{time},2N_{time}} \\ D_{N_{time}+1,N_{time}+1} & \cdots & D_{N_{time}+1,2N_{time}} \\ \cdots & \cdots & \cdots \\ D_{2N_{time},N_{time}+1} & \cdots & D_{2N_{time},2N_{time}} \end{bmatrix}
 \end{aligned} \tag{3.21}$$

$$[\phi]_{CL} = \begin{bmatrix} \phi_1 \\ \cdots \\ \phi_{N1} \end{bmatrix} ; \quad \left[ \frac{\partial \phi}{\partial n} \right]_{WET} = \begin{bmatrix} \frac{\partial \phi_{N1+1}}{\partial n} \\ \cdots \\ \frac{\partial \phi_{N_{time}}}{\partial n} \end{bmatrix} ; \quad [\phi]_{CU} = \begin{bmatrix} \phi_{N_{time}+1} \\ \cdots \\ \phi_{2N_{time}} \end{bmatrix} \tag{3.22}$$

where  $N1 = N_{time}-N_{wetmax}$

From continuity of perturbation potential at the trailing edge of the wetted part of the foil, (2.16) takes the discretized form of:

$$\phi_{N_{time}-N_{wetmax}} = \phi_{N_{time}-N_{wetmax}+1} \tag{3.23}$$

This is really only valid where the two panels intersect. A better numerical approximation, is to use the linear extrapolation:



$$\frac{\phi_{Ntime - Nwetmax + 2} - \phi_{Ntime - Nwetmax + 1}}{y_{Ntime - Nwetmax + 2} - y_{Ntime - Nwetmax + 1}} = \frac{\phi_{Ntime - Nwetmax + 1} - \phi_{Ntime - Nwetmax}}{y_{Ntime - Nwetmax + 1} - y_{Ntime - Nwetmax}} \quad (3.24)$$

But since we're using equal spacing, the denominators cancel out, and we're left with:

$$\phi_{Ntime - Nwetmax} = 2\phi_{Ntime - Nwetmax + 1} - \phi_{Ntime - Nwetmax + 2} \quad (3.25)$$

Making use of this continuity and assembling all the above modules, we obtain for the left hand side of the system of equations:

$$\begin{aligned} [S]_{CL} &= \begin{bmatrix} S_{1,1} & \dots & S_{1,Ntime - Nwetmax} \\ \dots & \dots & \dots \\ S_{Ntime,1} & \dots & S_{Ntime,Ntime - Nwetmax} \\ S_{Ntime + 1,1} & \dots & S_{Ntime + 1,Ntime - Nwetmax} \\ \dots & \dots & \dots \\ S_{2Ntime,1} & \dots & S_{2Ntime,Ntime - Nwetmax} \end{bmatrix} \\ [D]_{WET} &= \begin{bmatrix} J_1 & K_1 & D_{1,Ntime - Nwetmax + 3} & \dots & D_{1,Ntime - 1} & L_1 \\ \dots & \dots & \dots & \dots & \dots & \dots \\ J_{Ntime} & K_{Ntime} & D_{Ntime,Ntime - Nwetmax + 3} & \dots & D_{Ntime,Ntime - 1} & \dots \\ J_{Ntime + 1} & K_{Ntime + 1} & D_{Ntime + 1,Ntime - Nwetmax + 2} & \dots & D_{Ntime + 1,Ntime - 1} & \dots \\ \dots & \dots & \dots & \dots & \dots & \dots \\ J_{2Ntime} & K_{2Ntime} & D_{2Ntime,Ntime - Nwetmax + 2} & \dots & D_{2Ntime,Ntime - 1} & L_{2Ntime} \end{bmatrix} \\ [S]_{CU} &= \begin{bmatrix} S_{1,Ntime + 1} & \dots & S_{1,2Ntime} \\ \dots & \dots & \dots \\ S_{Ntime,Ntime + 1} & \dots & S_{Ntime,2Ntime} \\ S_{Ntime + 1,Ntime + 1} & \dots & S_{Ntime + 1,2Ntime} \\ \dots & \dots & \dots \\ S_{2Ntime,Ntime + 1} & \dots & S_{2Ntime,2Ntime} \end{bmatrix} \\ \left[ \frac{\partial \phi}{\partial n} \right]_{CL} &= \begin{bmatrix} \frac{\partial \phi_1}{\partial n} \\ \dots \\ \frac{\partial \phi_{Ntime - Nwetmax}}{\partial n} \end{bmatrix} ; [\phi]_{WET} = \begin{bmatrix} \phi_{Ntime - Nwetmax + 1} \\ \dots \\ \phi_{Ntime} \end{bmatrix} ; \left[ \frac{\partial \phi}{\partial n} \right]_{CU} = \begin{bmatrix} \frac{\partial \phi_{Ntime + 1}}{\partial n} \\ \dots \\ \frac{\partial \phi_{2Ntime}}{\partial n} \end{bmatrix} \end{aligned} \quad (3.27)$$

where in the  $Ntime-Nwetmax$  and in the  $Ntime$  column of the LHS we made the following substitution:

$$J_i = D_{i, Ntime - Nwetmax + 1} + 2D_{i, Ntime - Nwetmax} \quad ; \quad i=1 \dots 2Ntime \quad (3.28)$$

$$K_i = D_{i, Ntime - Nwetmax + 2} - D_{i, Ntime - Nwetmax} \quad ; \quad i=1 \dots 2Ntime \quad (3.29)$$

$$L_i = D_{i, Ntime} + D_{i, Ntime + 1} \left( \frac{y_{Ntime}}{y_{Ntime + 1}} \right) \quad ; \quad i=1 \dots 2Ntime \quad (3.30)$$

Consequently for the right hand side of the governing system of equations we obtain:

$$[D]_{CL} = \begin{bmatrix} D_{1,1} & \dots & D_{1, Ntime - Nwetmax} \\ \dots & \dots & \dots \\ D_{Ntime, 1} & \dots & D_{Ntime, Ntime - Nwetmax} \\ D_{Ntime + 1, 1} & \dots & D_{Ntime + 1, Ntime - Nwetmax} \\ \dots & \dots & \dots \\ D_{2Ntime, 1} & \dots & D_{2Ntime, Ntime - Nwetmax} \end{bmatrix} \quad (3.31)$$

$$[S]_{WET} = \begin{bmatrix} S_{1, Ntime - Nwetmax + 1} & \dots & S_{1, Ntime} \\ \dots & \dots & \dots \\ S_{Ntime, Ntime - Nwetmax + 1} & \dots & S_{Ntime, Ntime} \\ S_{Ntime + 1, Ntime - Nwetmax + 1} & \dots & S_{Ntime + 1, Ntime} \\ \dots & \dots & \dots \\ S_{2Ntime, Ntime - Nwetmax + 1} & \dots & S_{2Ntime, Ntime} \end{bmatrix}$$

$$[D]_{CU} = \begin{bmatrix} D_{1, Ntime + 1} & \dots & D_{1, 2Ntime} \\ \dots & \dots & \dots \\ D_{Ntime, Ntime + 1} & \dots & D_{Ntime, 2Ntime} \\ D_{Ntime + 1, Ntime + 1} & \dots & D_{Ntime + 1, 2Ntime} \\ \dots & \dots & \dots \\ D_{2Ntime, Ntime + 1} & \dots & D_{2Ntime, 2Ntime} \end{bmatrix}$$

$$[\Phi]_{CL} = \begin{bmatrix} \phi_1 \\ \dots \\ \phi_{Ntime - Nwetmax - 1} \\ 0 \end{bmatrix} ; \quad \left[ \frac{\partial \phi}{\partial n} \right]_{WET} = \begin{bmatrix} \frac{\partial \phi_{Ntime - Nwetmax + 1}}{\partial n} \\ \dots \\ \frac{\partial \phi_{Ntime}}{\partial n} \end{bmatrix} ; \quad [\Phi]_{CU} = \begin{bmatrix} 0 \\ \phi_{Ntime + 2} \\ \dots \\ \phi_{2Ntime} \end{bmatrix} \quad (3.32)$$

$$(3.33)$$

Notice that the  $N_{time}-N_{wetmax}$  element in the right hand side vector is zero. This is because its value is known and equal to the perturbation potential on the wetted trailing edge panel, and can thus be brought over to the left hand side of the equation. Similarly, since the perturbation potential on the cavity leading edge panel is equal to the perturbation potential on the wetted leading edge panel, it can be brought over to the left hand side and thus the  $N_{time}+1$  element in the right hand side vector is also zero.

But again as in the entry during phase I, the perturbation potentials on both the lower and upper cavity, at any time  $N_{time}$ , are known from the previous timesteps in the following matter:

$$\begin{aligned} \phi_j|_{time = N_{time}} &= \phi_{TE}|_{time = i} \quad ; \quad j = 1 \dots N_{cltime} - 1 \quad ; \quad i = N_{wetmax} \dots N_{time} - 2 \\ \phi_j|_{time = N_{time}} &= 0 \quad ; \quad j = N_{cltime} \end{aligned} \quad (3.34)$$

$$\begin{aligned} \phi_j|_{time = N_{time}} &= \phi_{LE}|_{time = i} \quad ; \quad j = N_{time} + 2 \dots 2N_{time} \quad ; \quad i = N_{time} - 1 \dots 1 \\ \phi_j|_{time = N_{time}} &= 0 \quad ; \quad j = N_{time} + 1 \end{aligned} \quad (3.35)$$

Finally, the right hand side vector can thus be written as:

$$\begin{aligned} [\Phi]_{CL} &= \begin{bmatrix} \phi_{TE}|_{l = N_{wetmax}} \\ \dots \\ \phi_{TE}|_{l = N_{time} - 2} \\ 0 \end{bmatrix} ; \quad \left[ \frac{\partial \phi}{\partial n} \right]_{WET} = \begin{bmatrix} \frac{\partial \phi_{N_{time} - N_{wetmax} + 1}}{\partial n} \\ \dots \\ \frac{\partial \phi_{N_{time}}}{\partial n} \end{bmatrix} ; \quad [\Phi]_{CU} = \begin{bmatrix} 0 \\ \phi_{LE}|_{l = N_{time} - 1} \\ \dots \\ \phi_{LE}|_{l = 1} \end{bmatrix} \end{aligned} \quad (3.36)$$

### 3.5 Non-Linear Cavity Shape Determination

At each timestep, as the foil enters through the free surface, the above system of equations is solved. Since a cubic B-spline curve is used to represent the arclength of the foil and cavity, as well as the perturbation potential distribution, the upper cavity is assumed to be on the foil surface for the first four timesteps. A similar method is used at the trailing

edge of the foil, when the foil is fully submerged. The lower cavity shape is assumed to be tangential to the trailing edge wetted panel, for the first three timesteps following complete submergence. Because of the singular behavior of the numerical solution near the free surface, the three panels on the lower cavity closest to the free surface are never aligned iteratively. Rather they are aligned tangentially to the preceding panels. Aside from these exceptions, used to implement the numerical model, the alignment of the cavity shape is found iteratively, such that (2.14) is satisfied. The discretized form of equation (2.19) takes the form:

$$h_{i+1} = h_i \cdot \left( \frac{q_n}{q_s} \Delta s \right) \Big|_i \quad (3.37)$$

where  $q_n$  and  $q_s$  are the normal and tangential velocities to the cavity respectively, and  $\Delta s$  is the arc length of the panel. The correction to the cavity height,  $h$ , is calculated at each iteration per timestep, and is then added normal to the current cavity surface, at each panel edge, as sketched out in Figure 3.6

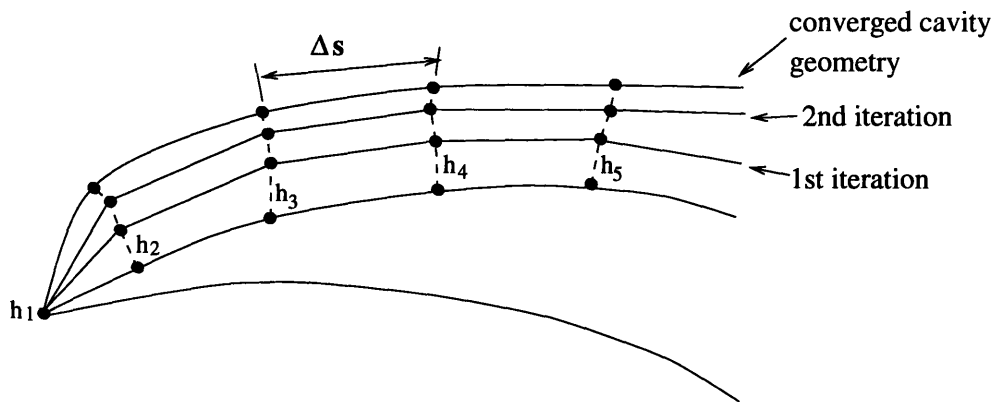


**Figure 3.6** Iterative cavity surface determination

At each timestep, equations (3.17) and (3.37) are solved until convergence of the cavity geometry is attained or  $q_n=0$ . Usually, no more than 2 or 3 iterations per timestep are needed for convergence.

### 3.6 Pressures on the Foil

The potential distribution along the foil and cavity, needed for the pressure distribution calculations, are known either from the solution of the governing set of equations or directly from the boundary conditions. On the wetted part of the foil, the perturbation potential on each panel, comes directly from the solution in matrix form. For the first phase, the initial entry, the indexing of the solution corresponding to the perturbation potential is:

$$[\phi]_{WET} = \begin{bmatrix} \phi_1 \\ \dots \\ \phi_{Ntime} \end{bmatrix} \quad (3.38)$$

For the second phase, the fully submerged case, the indexing is as follows:

$$[\phi]_{WET} = \begin{bmatrix} \phi_{Ntime - Nwetmax + 1} \\ \dots \\ \phi_{Ntime} \end{bmatrix} \quad (3.39)$$

The total potential at each panel control point is calculated by adding the inflow potential, defined by (2.5), to the results of the solution above.

The surface velocities,  $q_B$ , are computed by splining the total potentials,  $\Phi$ , in a piecewise parabolic distribution and then taking the spatial derivative. The total potential is given by:

$$\Phi = \phi + U_{\infty}y \quad (3.40)$$

The steady component of the pressure is then simply  $1 - (q_B)^2$

The unsteady component of the pressure,  $\frac{\partial\phi}{\partial t}$  due to the change in potential on each panel with time, is found by approximating the time derivative via a finite difference scheme in terms of the perturbation potential from the last three timesteps. The vectors (3.38) and (3.39) are stored in memory for the last three timesteps for this purpose. Finally the total pressure distribution is found by applying (2.25) at each panel control point.



# Chapter 4

## Numerical Validation

### 4.1 Convergence

#### 4.1.1 Convergence with Iterations per Timestep

At each timestep the governing system of equations is solved and the cavity geometry is found iteratively. Figure 4.1 shows the correction to the cavity surface from each iteration per timestep at the end of the initial entry phase, when the foil trailing edge is flush with the free surface. When the cavity growth is less than  $10^{-5}$ , it can be considered that convergence of cavity geometry is achieved. In other words, equation (2.14) is satisfied, the flow is tangential along the cavity surface.

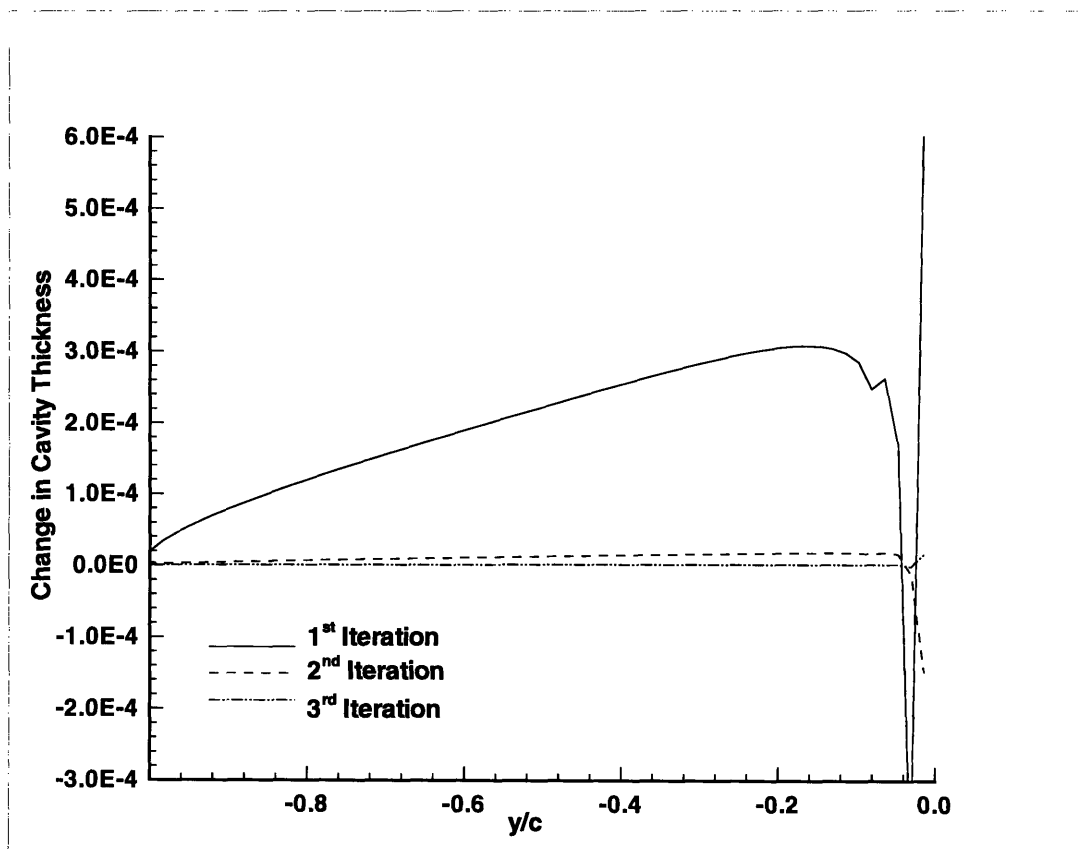


**Figure 4.1** Convergence of upper cavity thickness growth with iterations per timestep. Foil geometry is a flat plate at  $\alpha = 5^\circ$ ,  $d/c = 1.0$ , 120 panels discretization.



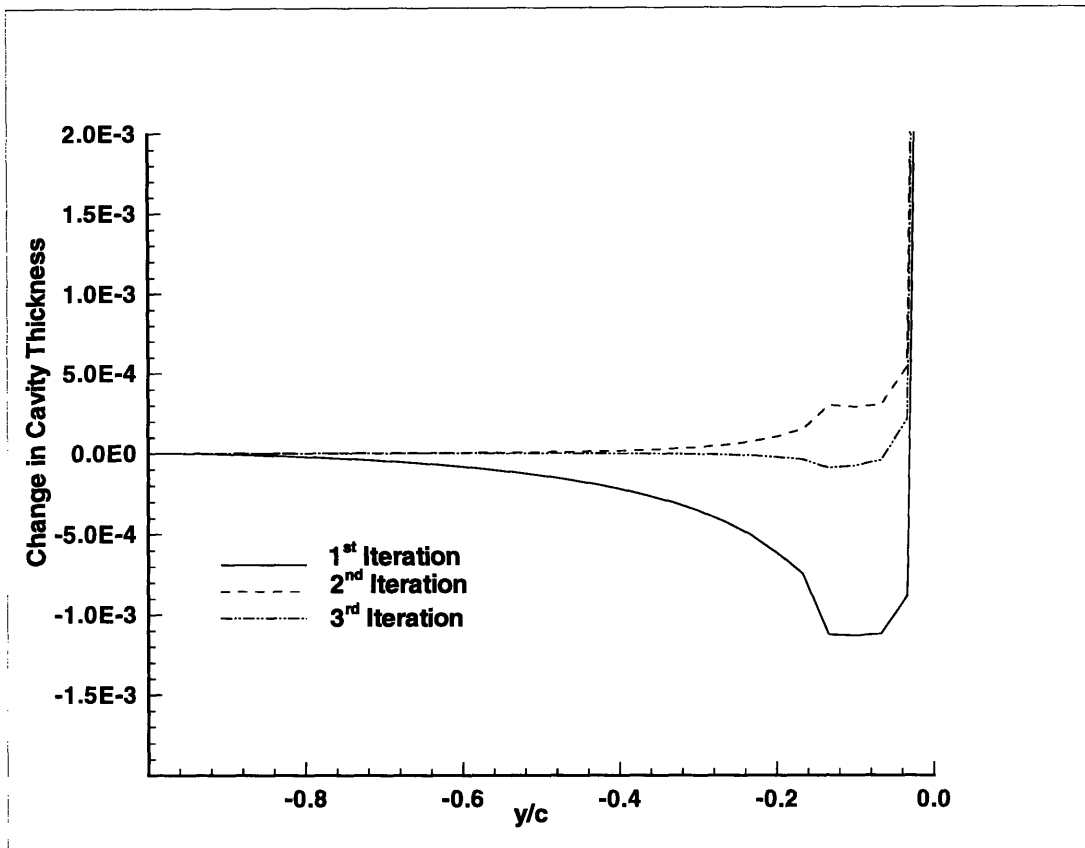


**Figure 4.2** Convergence of lower cavity thickness growth with iterations per timestep. Foil geometry is a flat plate at  $\alpha = 5^\circ$ ,  $d/c = 2.0$ , 60 panels discretization.

The developed numerical method is shown to converge very rapidly with iterations per timestep, and is reflected in the overall cavity thickness geometry shape, shown in Figure 4.3, and Figure 4.4. Notice that the present theory breaks down at the intersection with the free surface, shown in Figure 4.1 and Figure 4.2, due to a local singularity, that the paneling cannot resolve.

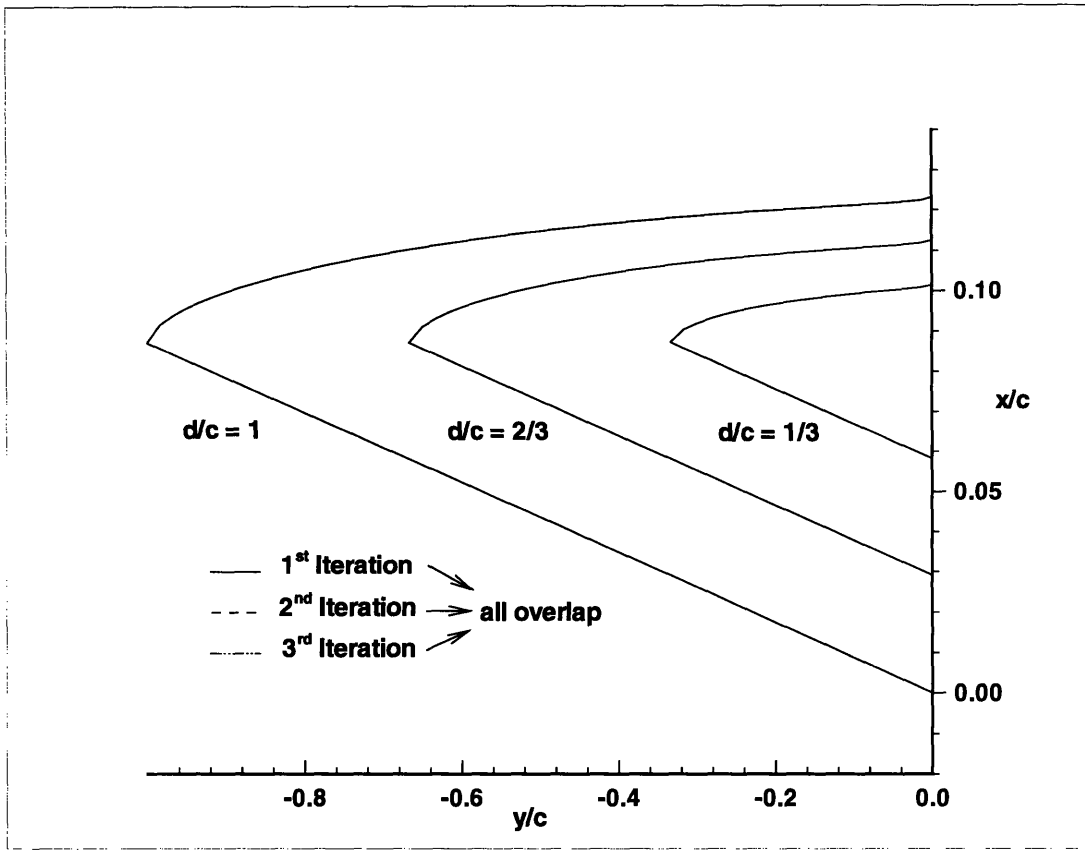


**Figure 4.3** Cavity geometry convergence with iterations per timestep.  
 Foil geometry is a flat plate at  $\alpha = 5^\circ$ , initial entry phase, 120 panels discretization.

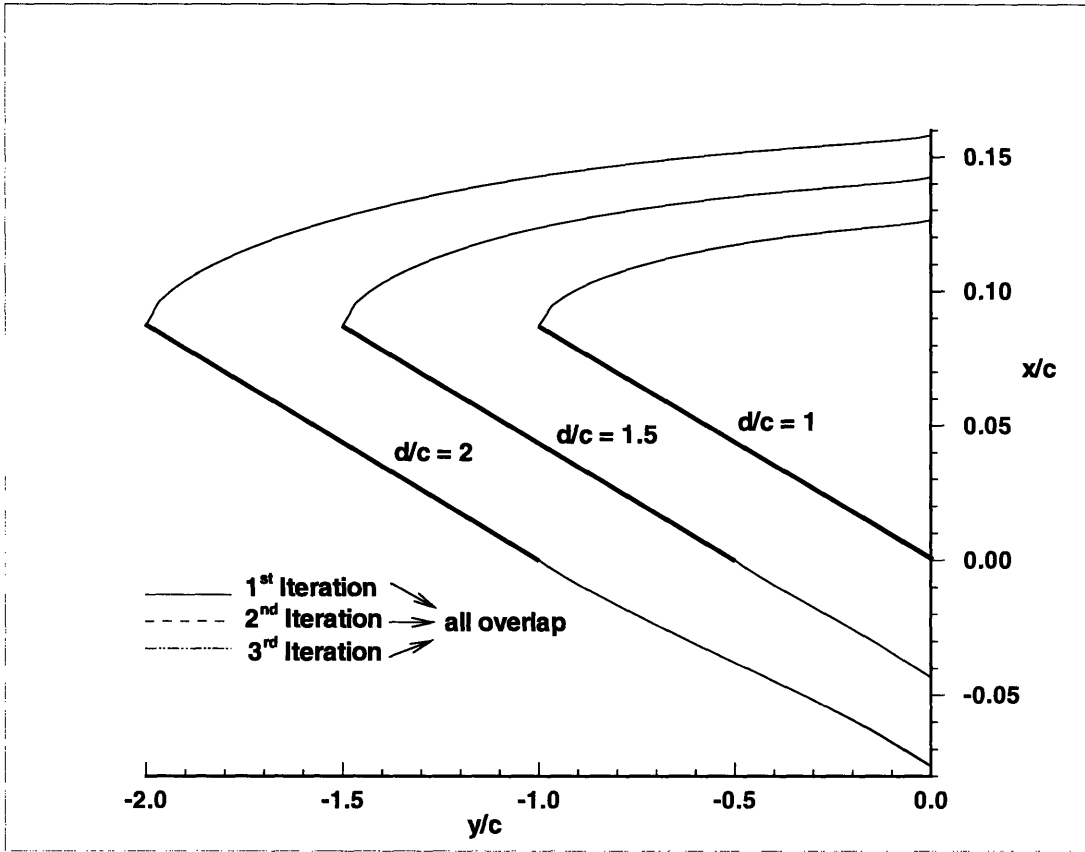


**Figure 4.4** Cavity geometry convergence with iterations per timestep.  
 Foil geometry is a flat plate at  $\alpha = 5^\circ$ , complete entry phase, 60 panels discretization.

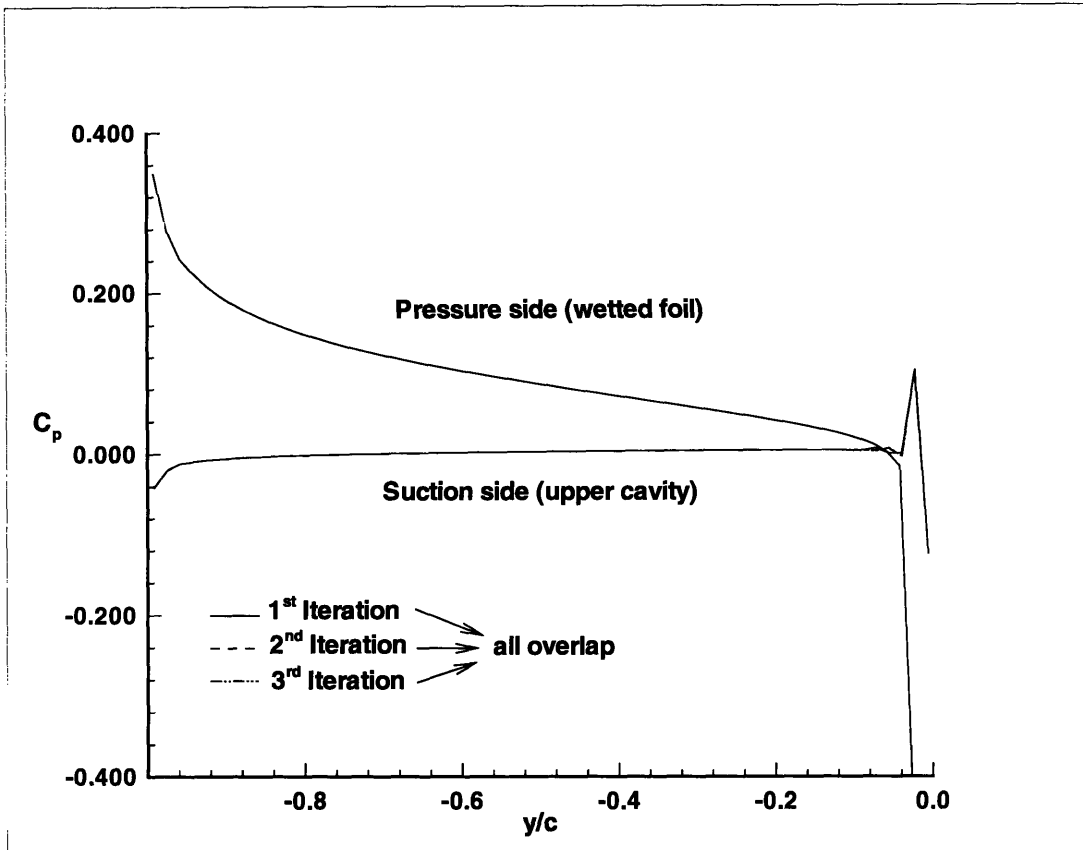


**Figure 4.5** Pressure distribution convergence with iterations per timestep. Foil geometry is a flat plate at  $\alpha = 5^\circ$ ,  $d/c = 1.0$ , 120 panels discretization.

The pressure distribution is also shown to converge very well with increasing number of iterations per timestep, as shown in Figure 4.5. The pressure distribution on the suction side cavity is shown to converge to zero value, as should be expected, since the pressure inside the ventilated cavity equals atmospheric pressure. Again, there is a numerical singular behavior near the free surface,  $y/c = 0$ , that the panel discretization cannot capture entirely. Notice also, in Figure 4.6, there is a discretization error, in that the panel method tries to capture the transition region near the trailing edge of foil and lower cavity, around  $y/c = -1.0$ , where the pressure along the foil must become zero along the cavity.

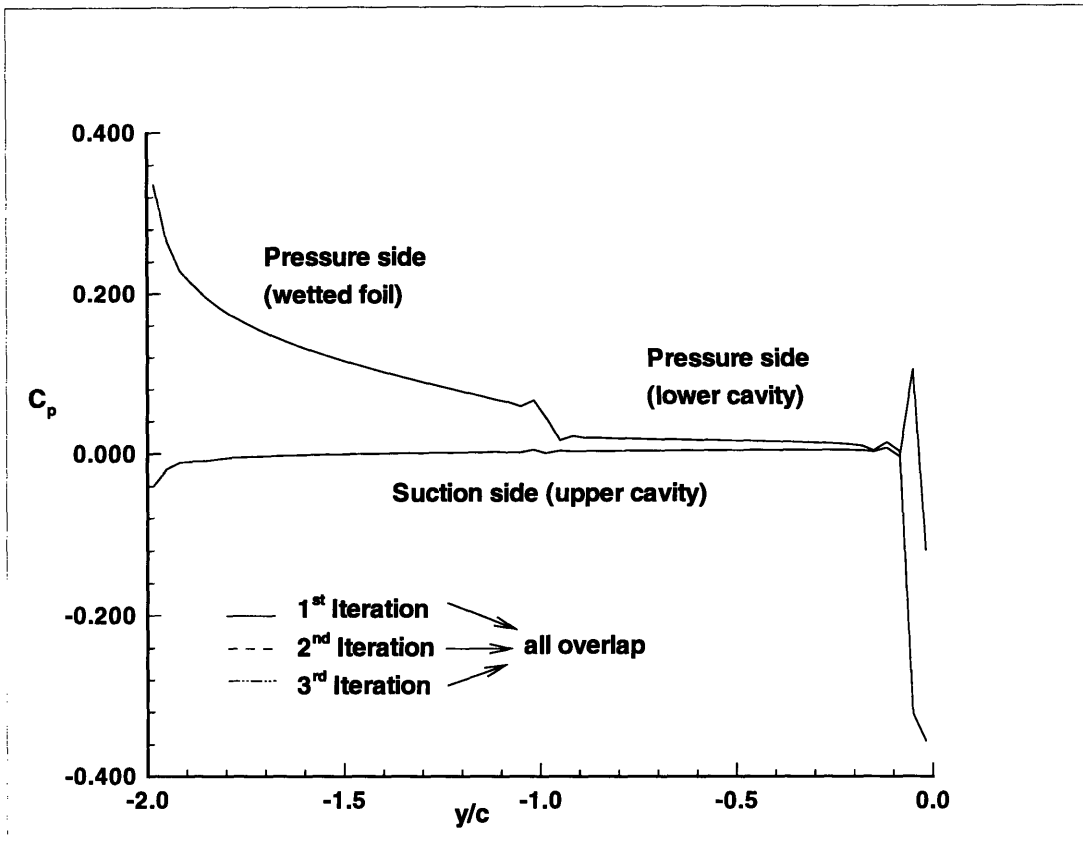


**Figure 4.6** Pressure distribution convergence with iterations per timestep. Foil geometry is a flat plate at  $\alpha = 5^\circ$ ,  $d/c = 2.0$ , 60 panels discretization.

#### 4.1.2 Convergence with Panel Discretization

Figure 4.7 shows the cavity geometry convergence with number of panels. It appears that the overall cavity shape converges slowly with number of panels, even though the difference in cavity shapes for increasing number of panels are not as large. This is primarily due to the fact that the panel arrangement at the leading edge is dictated by the constant time step approach, as shown in Figure 4.8.

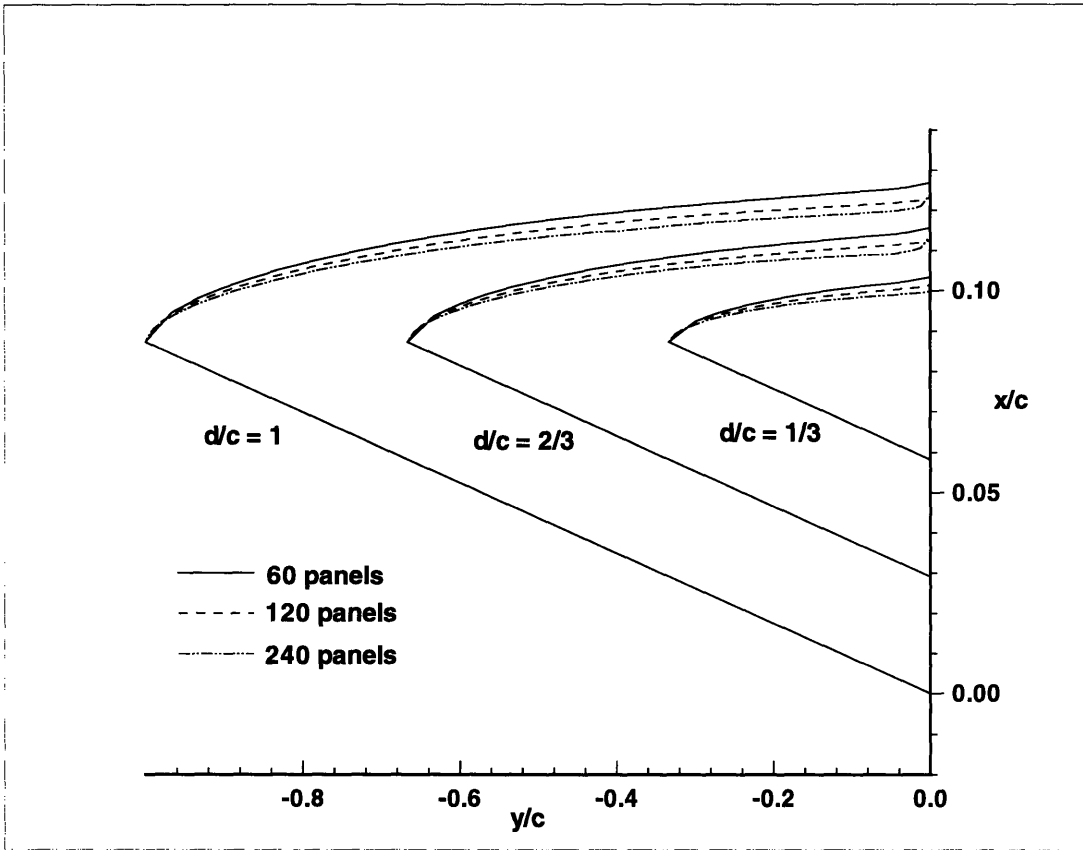


**Figure 4.7** Cavity geometry convergence with panel discretization. Foil geometry is a flat plate at  $\alpha = 5^\circ$ . Three iterations per timestep.

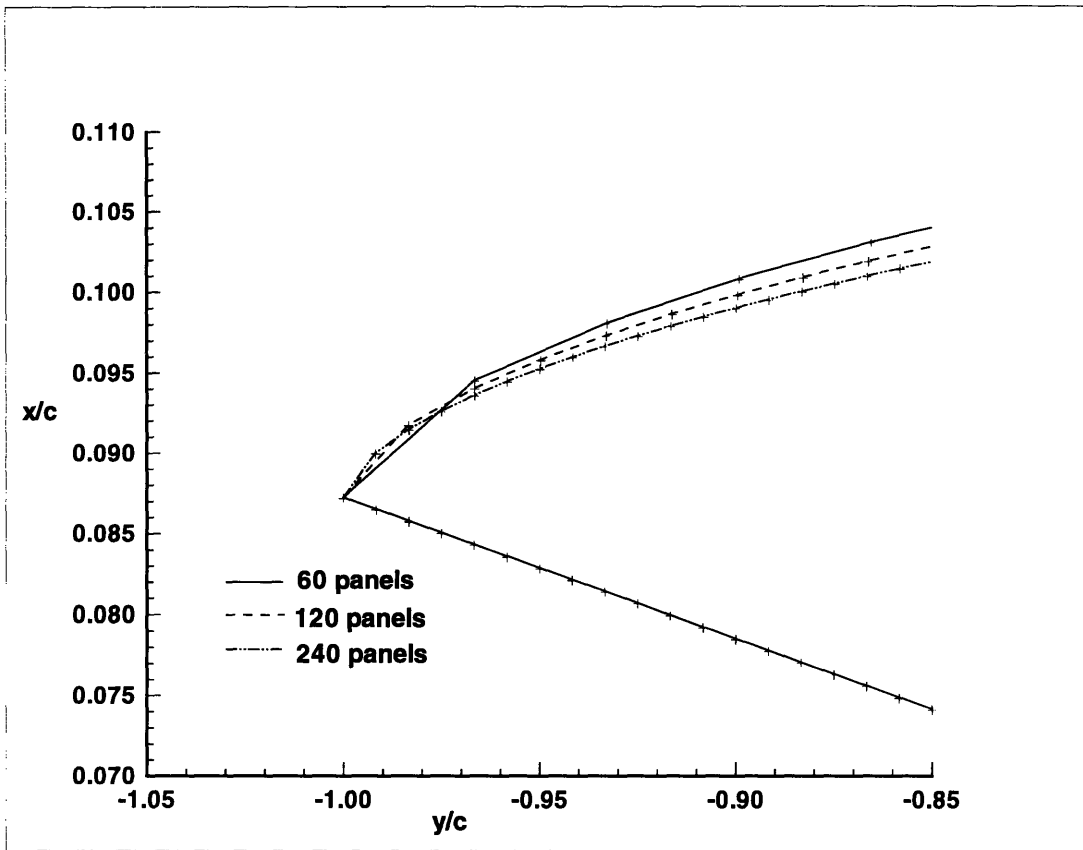


**Figure 4.8** Sensitivity of cavity geometry convergence to leading edge paneling. Foil geometry is a flat plate at  $\alpha = 5^\circ$ . Three iterations per timestep.

This does however not affect the overall pressure forces acting on the foil and the cavity, as can be seen in Figure 4.9. Notice again, that even a very fine panel discretization does not fully capture and resolve the singular behavior near the free surface. The singular behavior however affects a narrower region with increased panelling.

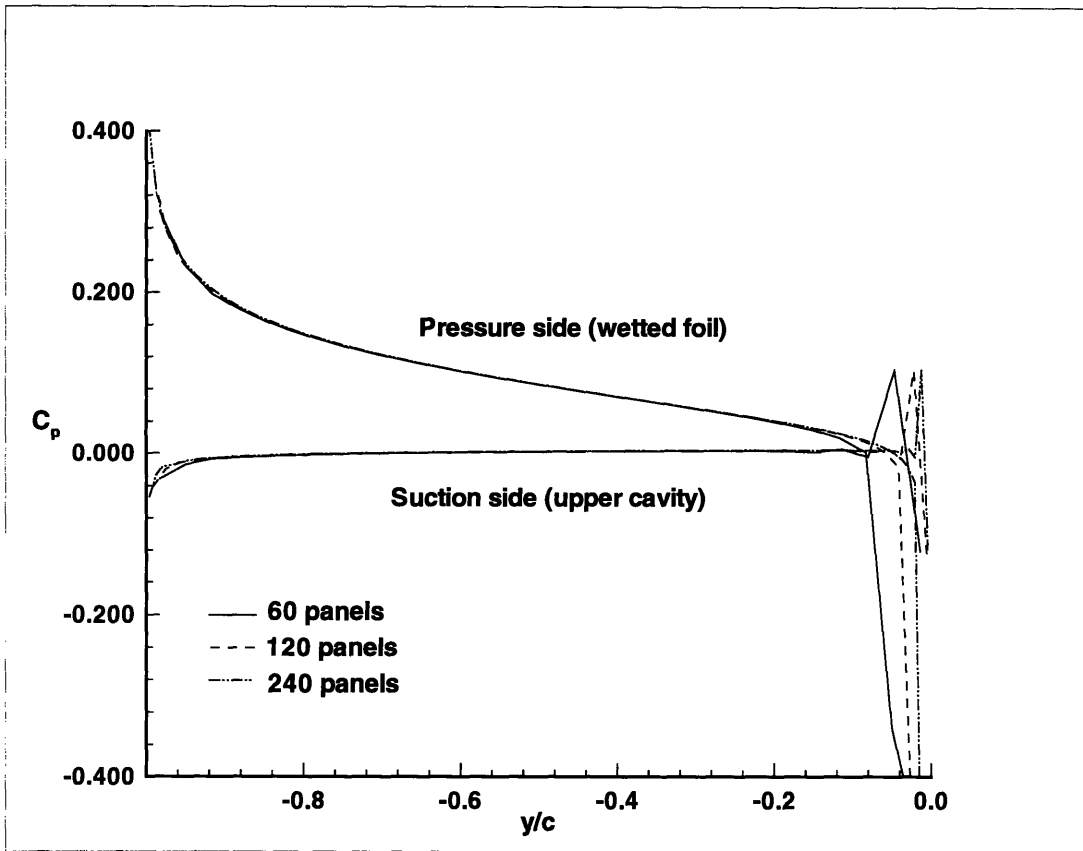


**Figure 4.9** Pressure distribution convergence with panel discretization. Foil geometry is a flat plate at  $\alpha = 5^\circ$ . Three iterations per timestep.

By comparing the results in Figure 4.5 with the results in Figure 4.9, as well as the CPU times shown in Table 4.1, we can conclude that it is computationally more efficient to do the analysis with a moderate panel discretization and several iterations per timestep, as shown in Figure 4.10, rather than using a very fine panel discretization and only one or two iterations per timestep, as shown in Figure 4.11. This is due to the fact that the CPU time roughly scales with the number of panels squared.



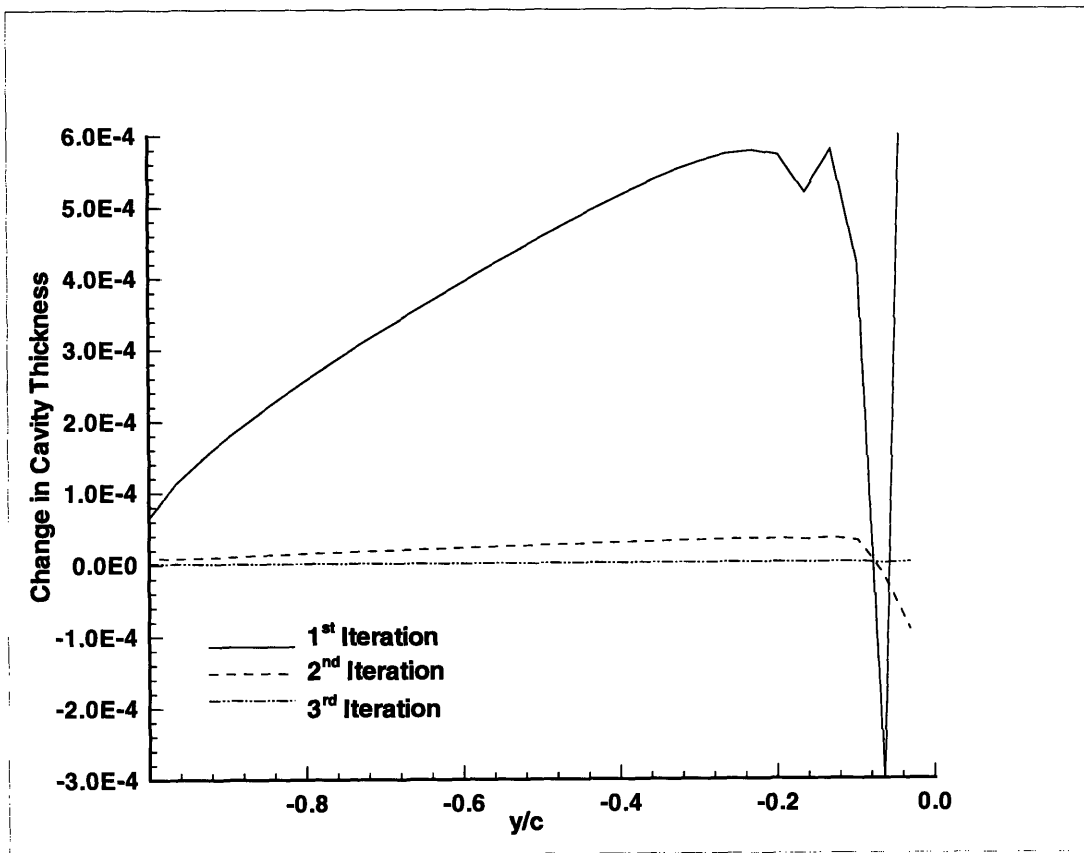


**Figure 4.10** Convergence of cavity thickness growth with iterations per timestep. Foil geometry is a flat plate at  $\alpha = 5^\circ$  with 60 panels discretization.

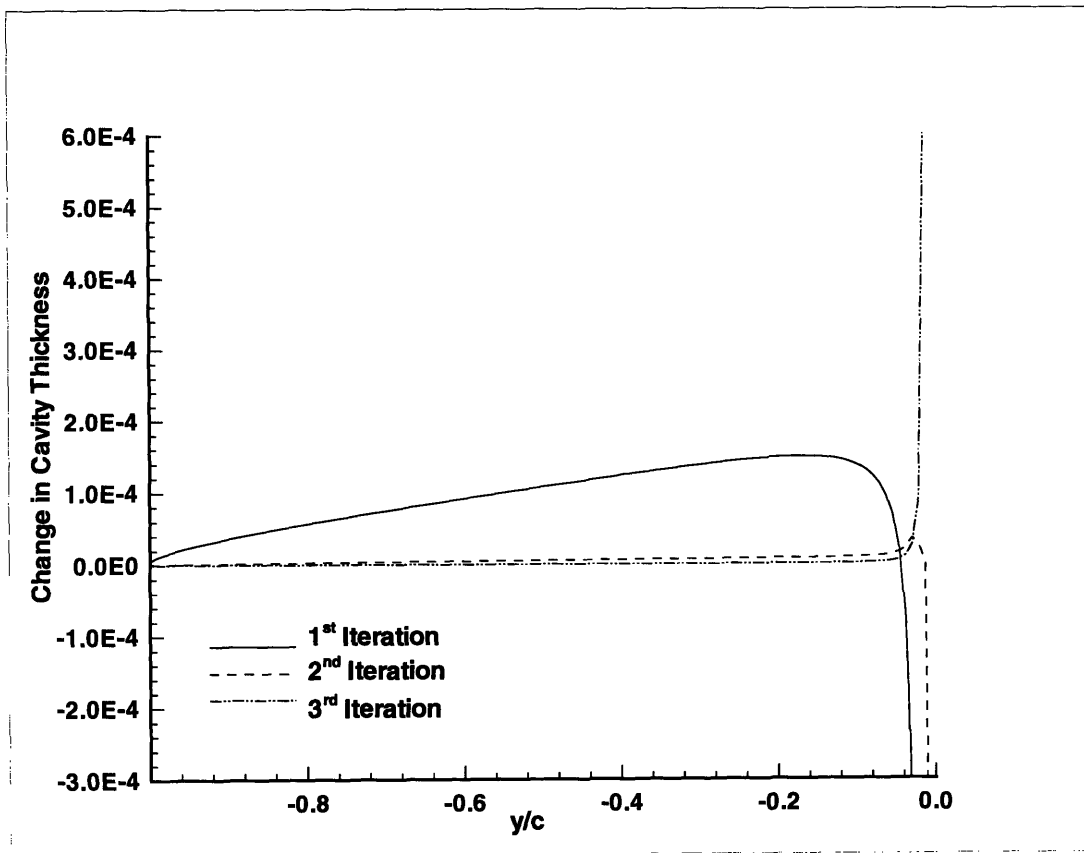


**Figure 4.11** Convergence of cavity thickness growth with iterations per timestep.  
 Foil geometry is a flat plate at  $\alpha = 5^\circ$  with 240 panels discretization.

Panel Discretization	1 iteration/ timestep	2 iterations/ timestep	3 iterations/ timestep
60 panels	2 sec	4 sec	6 sec
120 panels	10 sec	20 sec	30 sec
240 panels	70 sec	140 sec	210 sec

**Table 4.1 :** CPU times for analysis of flat plate geometry at  $\alpha = 5^\circ$  on a DEC Alphastation 600 5/266.

## 4.2 Comparisons with Other Methods

B. Yim and D.P. Wang used conformal mapping techniques to address the linearized problem of surface piercing hydrofoils. Figure 4.12 shows there is a very large difference between the linear, using Yim's model, and the non-linear cavity shape. This is mainly due to the fact that Yim assumes the flow to be symmetric about the foil and cavity.

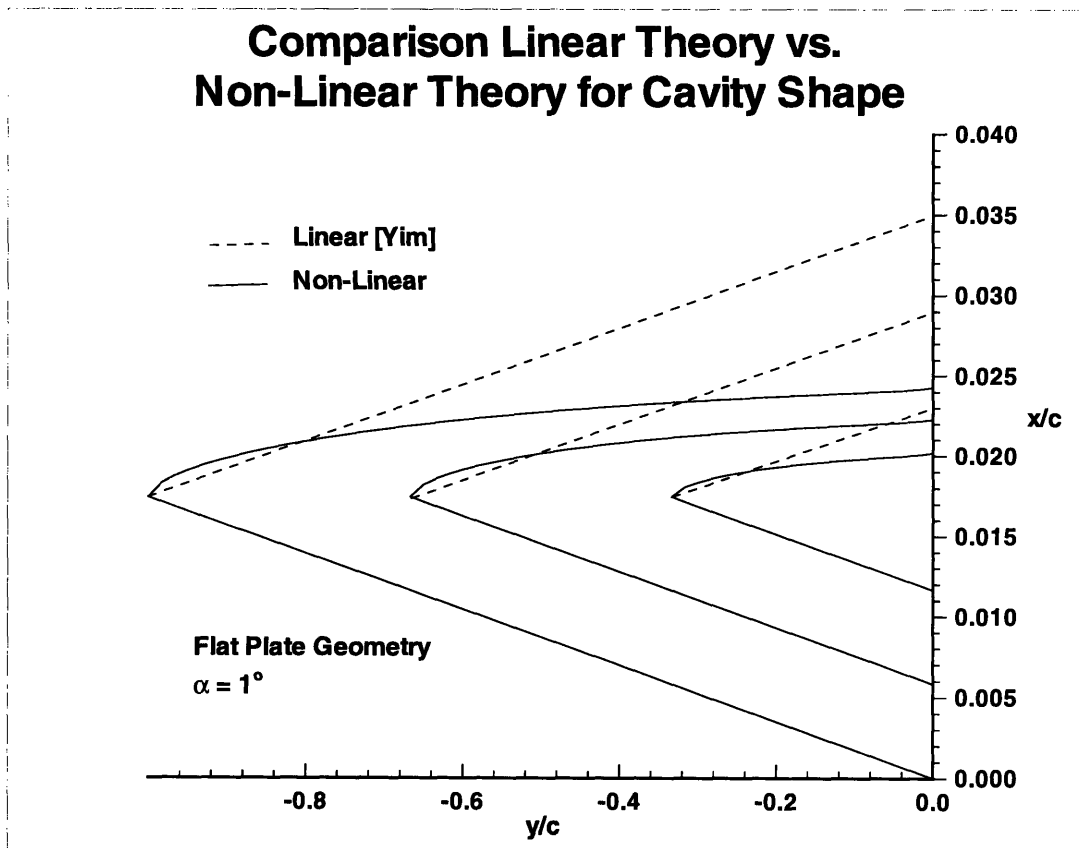


**Figure 4.12** Comparison of Linear Cavity Shape and Non-Linear Cavity Shape  
Foil geometry is a flat plate at  $\alpha = 1^\circ$  with 240 panels discretization

The linear analytical calculations of the pressure distribution on a surface piercing flat plate at small angles of attack, are compared to the current method for different depth of submergence. The non-linear pressure distribution near the free surface was splined and

then extrapolated to the exact free surface position to generate a smooth profile for comparisons.

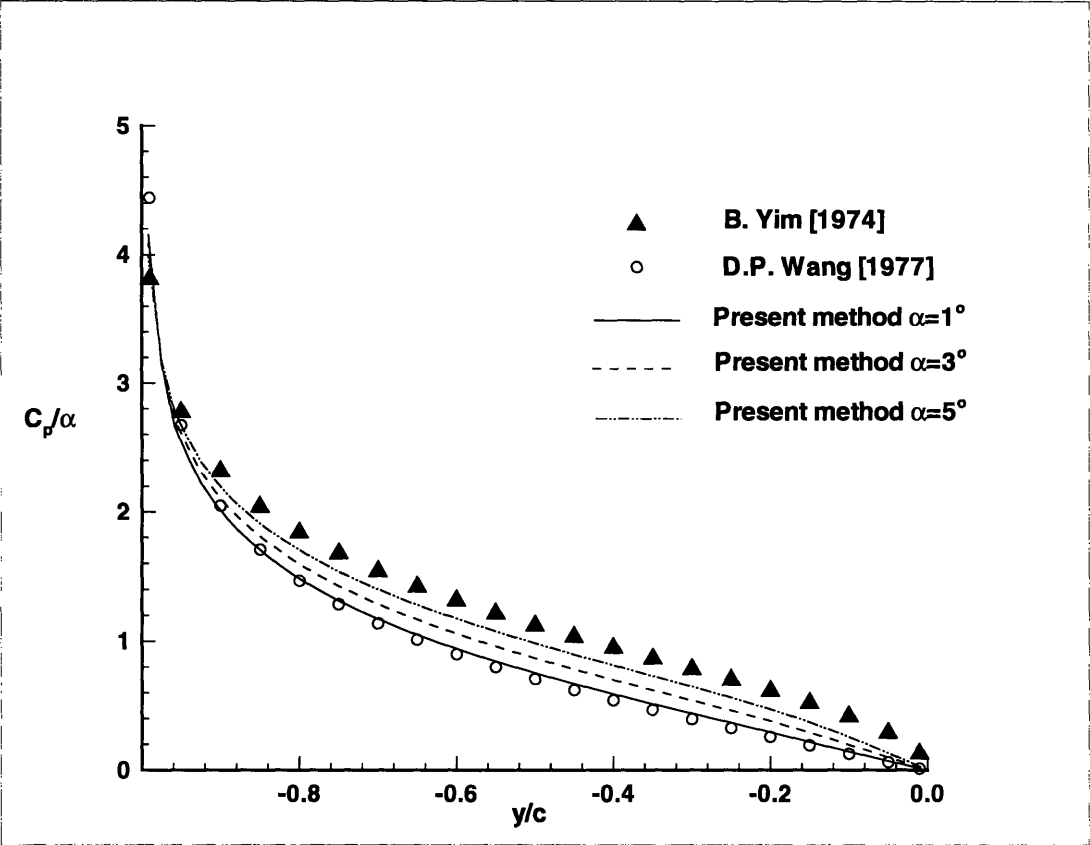


**Figure 4.13** Comparison of Linear Theory and Non-Linear Theory for Pressure Distribution on the Pressure Side of a Flat Plate at  $d/c = 1.0$

The current non-linear method compares very well with Wang’s linear analytical results at small angles of attack for the flat plate case, as shown in Figure 4.13. This is mainly due to the fact that Wang allows for asymmetry of the cavity and blade geometry, as opposed to Yim, who assumes the flow to be symmetric about the foil and cavity. Wang’s method thus more closely relates to the present method, except of course for the non-linear cavity effects. However, for completeness, the results from Yim will also be included in the comparisons.

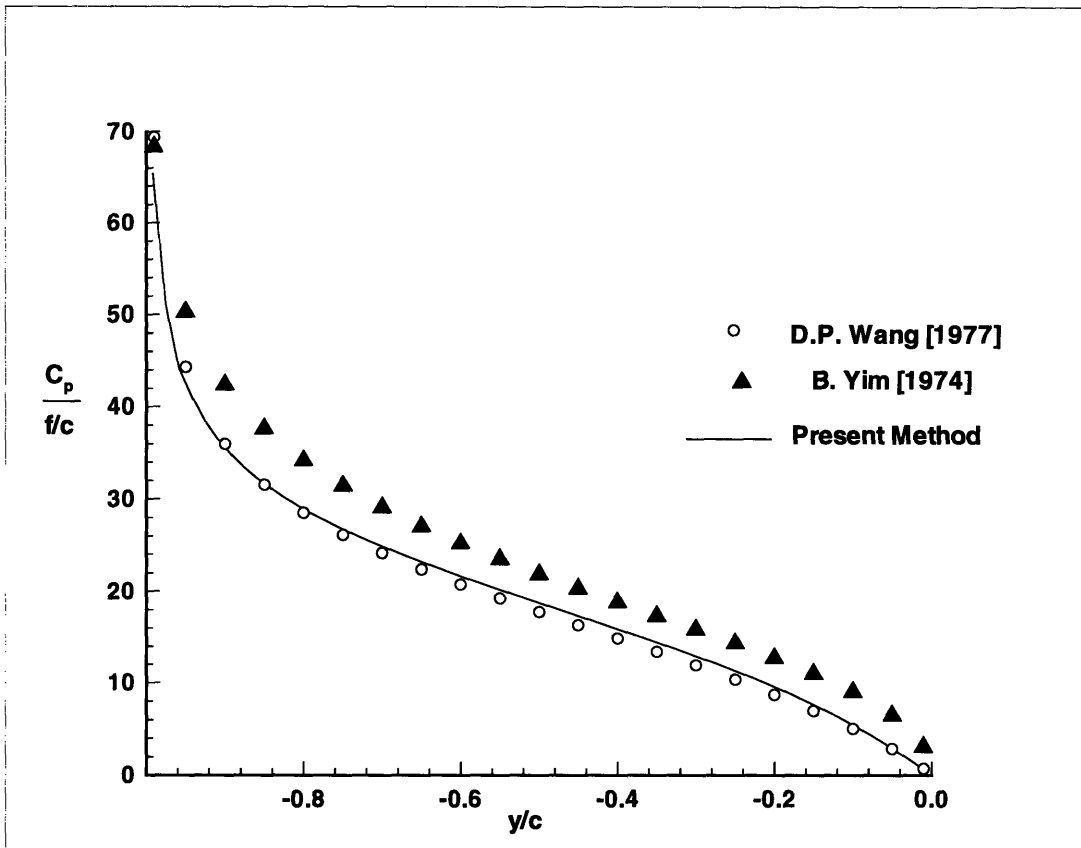


**Figure 4.14** Comparison of Linear and Non-Linear Theory for Pressure Distribution. Parabolically Cambered Foil.  $f/c = 0.001$ ,  $\alpha = 1^\circ$  with 120 panels discretization

The effects of camber are investigated for a parabolic camber profile in Figure 4.14 through Figure 4.16. At low camber to chord ratios, the present method agrees favorably with the linearized theory of Wang. Yim's method seems to overpredict the pressures. Again, this is most likely due to the inherent assumption in Yim's theory, that the flow is symmetric about the foil and cavity.

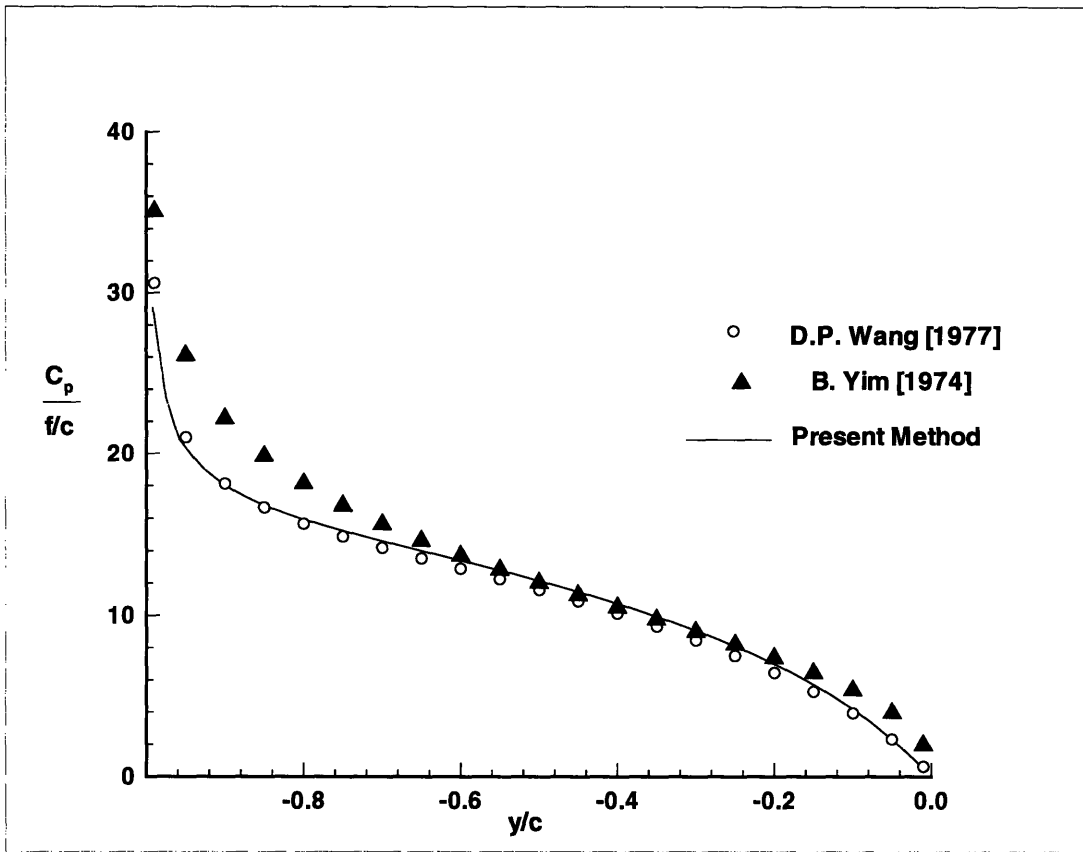


**Figure 4.15** Comparison of Linear and Non-Linear Theory for Pressure Distribution. Parabolically Cambered Foil.  $f/c = 0.002$ ,  $\alpha = 1^\circ$  with 120 panels discretization

As the camber increases, the difference between the linear and non-linear methods become more apparent, although at a slower rate than increased angle of attack. Wang's method seems to show the correct trend, but Yim's method seems however to deteriorate for more cambered foils.

The difference in magnitude between the linear and non-linear results, will of course become even more apparent for combined high angle of attack and cambered foils. The pressure loading can indeed be divided in two parts: (1) effects of angle of attack, as

shown in Figure 4.13 and (2) camber effects, as shown in the above figure and the one following next.

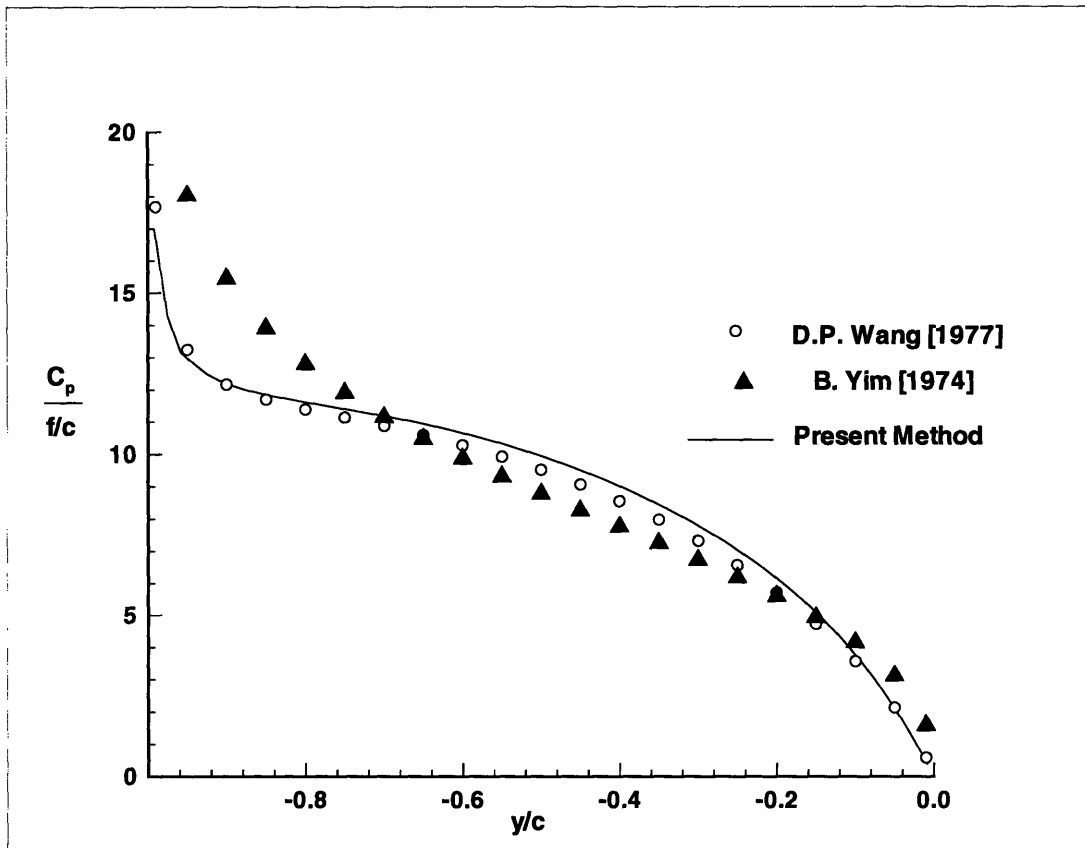


**Figure 4.16** Comparison of Linear and Non-Linear Theory for Pressure Distribution. Parabolically Cambered Foil.  $f/c = 0.003$ ,  $\alpha = 1^\circ$  with 120 panels discretization

Physically, for highly cambered foils operating at low angles of attack, a ventilated cavity might originate on the lower suction side of the foil. This would have an essential effect on the direction of the lift and drag forces. This behavior cannot be captured with the present method.

# Chapter 5

## Conclusions and Recommendations

### 5.1 Conclusions

A non-linear, time-marching, potential based boundary element method was developed for the analysis of flow around a surface piercing two-dimensional hydrofoil of arbitrary geometry. The method is used for the two phases (initial entry and full submergence) of the foil's trajectory through the free surface, and is successfully implemented for the initial entry phase and the fully submerged phase. The method converges very rapidly for the unknown cavity geometry, with number of iterations per timestep and increasing panel resolution. The final cavity shape is sensitive to the cavity discretization near the leading edge. The pressure distribution along the foil and cavity remains almost unchanged after the first iteration, and is not very sensitive to the leading edge cavity shape. Comparisons of the developed method with Yim's linear analytical method show that there is a very large difference in cavity geometry. This is because of a basic assumption made in Yim's linear theory, that the flow is symmetric about the foil. The non-linear cavity shapes are much smaller. The pressure distributions compare very well for flat plate geometries at small angles of attack and for parabolically cambered foils with small camber to chord ratios. At higher angles of attack, and/or increasing camber, the non-linear effects become much more apparent.

Although the presented method is two-dimensional, it still provides a good estimate of the flow around each span wise cut of a surface piercing or partially submerged propeller. Strictly considered, full motion of a partially submerged propeller consists of the initial entry phase, followed by the complete entry phase and finally the exit phase. However during the propeller blade's exit, the loading vanishes as it cuts back through the free sur-



face. Therefore, the exit phase is not critical in predicting the overall hydrodynamic forces generated on a surface piercing blade. The most important phase is clearly the initial entry, since the loading on the propeller blade, very rapidly increases to its full value from zero loading. The herein developed two-dimensional method which is very efficient at predicting the cavity geometry and pressure distributions during the entry phase, and can thus be used as a basis to design surface piercing propeller blades.

## **5.2 Recommendations and Future Work**

The sensitivity of the converged overall cavity shape, to the leading edge cavity geometry, suggests that a finer panel arrangement locally at the leading edge might further improve the overall converged cavity shape. As shown in this work, this modification will have negligible effect on the pressure distribution. A finer panel arrangement near the free surface panels, might also improve the singular pressure behavior. It is therefore recommended that a cosine spaced, instead of the actual even spaced, panel arrangement be implemented in the future. This modification will however increase the computational time and complexity of the code, as the perturbation potentials will need to be splined, interpolated and extrapolated to their new panel location at each timestep.

Another area of possible improvements are the leading edge region and the foil trailing edge/cavity regions. To better satisfy continuity at those points, the perturbation potentials will again need to be splined and extrapolated to those exact locations. In the same region, the pressure distribution might be improved by using a transition zone, over which the pressure is allowed to smoothly pass from the value on the wetted foil, to zero value on the trailing cavity side. This will inherently change the structure of the governing system of equations. For completeness of the full problem analysis of the surface piercing foil, the modeling of the exit phase should also be considered, however small its effect might be on the overall performance characteristics.

An area not touched upon in this work, is the calculation of the forces. These can be evaluated by integrating the computed pressure distributions, and could easily be implemented. From these, the vibration forces can be calculated. Equally important as the hydrodynamics of the problem, are the hydro-elastic effects. The time evolution of the forces during the entry phase are indeed very large, and could alter the foil geometry significantly enough to have a hydrodynamic effect. Hence, to fully represent the physics of the surface piercing foil, a structural coupling model with the hydrodynamic analysis is needed.



## References

- [1] B.D. Cox. Hydrofoil Theory for Vertical Water Entry. Ph.D. Thesis, M.I.T., Cambridge, Mass., 1971.
- [2] N.E. Fine, S.A. Kinnas. A boundary Element Method for the Analysis of the Flow Around Three-Dimensional Cavitating Hydrofoils. *Journal of Ship Research*. Vol. 37, No. 3, September 1993, pp 213-224.
- [3] O. Furuya A Performance Prediction Theory for Partially Submerged Ventilated Propellers. *Fifteenth Symposium on Naval Hydrodynamics*, Hamburg, Germany, 1984.
- [4] J.B. Hadler ad R Hecker. Performance of Partially Submerged Propellers. *Seventh Symposium of Naval hydrodynamics*, Rome, Italy, 1968 pp 1449-1496.
- [5] S.A. Kinnas and N.E. Fine. Non-Linear Analysis of the Flow Around Partially or Super-Cavitating Hydrofoils by a Potential Based Panel Method. In *Boundary Integral Methods - Theory and Applications, Proceedings of the IABEM-90 Symposium of the International Association for Boundary Element Methods*, pp 289-300, Rome, Italy, October 1990, Springer-Verlag.
- [6] S.A. Kinnas and N.E. Fine. A Numerical Non-Linear Analysis of the Flow Around Two-Dimensional and Three-Dimensional Partially Cavitating Hydrofoils. *Journal of Fluid Mechanics*. Vol. 254, 1993, pp 151-181.
- [7] N. Olofsson. A Contribution on the Performance of Partially Submerged Propellers. FAST'93, Yokohama, Japan, December 13-16, 1993.
- [8] W.S. Vorus. Forces on Surface-Piercing Propellers with Inclination. *Journal of Ship Research*. Vol. 35, No. 3, September 1991, pp 210-218.
- [9] D.P. Wang. Water Entry and Exit of a Fully Ventilated Foil. *Journal of Ship Research*. Vol. 21, No. 1, March 1977, pp 44-48.
- [10] D.P. Wang. Oblique Water Entry and Exit of a Fully Ventilated Foil. *Journal of Ship Research*. Vol. 23, No. 1, 1979, pp 43-54.
- [11] B. Yim. Linear Theory on Water Entry and Exit Problems of a Ventilating Thin Wedge. *Journal of Ship Research*. Vol. 18, No. 1, March 1974, pp 1-11.